Published in final edited form as:
Eur J Nucl Med Mol Imaging. 2011 February ; 38(2): 358–377. doi:10.1007/s00259-010-1569-z.

Molecular imaging in cancer treatment

Mark H. Michalski and
Stanford University School of Medicine, Stanford, CA 94305, USA

Xiaoyuan Chen
Laboratory of Molecular Imaging and Nanomedicine (LOMIN), National Institute of Biomedical Imaging and Bioengineering (NIBIB), National Institutes of Health (NIH), 31 Center Drive, Suite 1C14, Bethesda, MD 20892-2281, USA, shawn.chen@nih.gov

Abstract

The success of cancer therapy can be difficult to predict, as its efficacy is often predicated upon characteristics of the cancer, treatment, and individual that are not fully understood or are difficult to ascertain. Monitoring the response of disease to treatment is therefore essential and has traditionally been characterized by changes in tumor volume. However, in many instances, this singular measure is insufficient for predicting treatment effects on patient survival. Molecular imaging allows repeated in vivo measurement of many critical molecular features of neoplasm, such as metabolism, proliferation, angiogenesis, hypoxia, and apoptosis, which can be employed for monitoring therapeutic response. In this review, we examine the current methods for evaluating response to treatment and provide an overview of emerging PET molecular imaging methods that will help guide future cancer therapies.

Keywords

Molecular imaging; Therapy response; Metabolism; Proliferation; Angiogenesis; Hypoxia; Apoptosis

Introduction

The potential of molecular imaging, which allows the visualization of fundamental biomolecular and cellular processes, is both vast and largely unrealized. Nevertheless, molecular imaging at the preclinical level has already led to a greater understanding of the pathophysiologic mechanisms that underpin neoplasm and may eventually promote more effective drug development through early target validation, pharmacodynamic monitoring, and target patient selection. The development of molecular imaging in the clinical setting has only just begun and could yield tremendous patient benefit in the form of earlier lesion detection, treatment response monitoring, and a truly individualized approach to treatment of cancer.

Much of the impetus behind “personalized medicine” in oncology is based on the weakness of current therapeutic options. Standard therapies for neoplasm characteristically suffer from low response rates and substantial side effects due to systemic toxicity, particularly in the treatment of disseminated solid tumors. The promise of a personalized approach is tied to

Correspondence to: Xiaoyuan Chen.

Conflicts of interest None.

improving these therapies through uncovering the underlying molecular and cellular patho-physiologic processes that dictate therapeutic susceptibility. Early efforts in personalized medicine have resulted in targeted, pathway-specific therapeutics and, along with them, the possibility of discovering and tailoring treatments based on individual tumor susceptibilities. In vitro studies of neoplastic tissue receptor expression and single gene mutations for pretreatment testing is commonplace in breast cancer, where testing for human epidermal growth factor receptor (EGFR) 2 (HER2) overexpression is measured to determine trastuzumab treatment susceptibility [1]. Similarly, testing for KRAS gene variants is required for testing EGFR antibody susceptibility and can additionally yield critical information in the use of EGFR kinase inhibitors [2,3].

While there have been some early successes in leveraging diagnostics for improved treatment, current in vitro tests reflect only a part of the underlying cancer biology that leads to drug susceptibility; this is reflected, for example, in the 50% of HER2-overexpressing breast cancers that do not respond to trastuzumab [4]. Advanced proteomic analysis, gene expression, and genome sequencing approaches are making headway in transitioning from the research setting to the clinical laboratory, but still need extensive validation before being clinically utilized to develop personalized therapies. Additionally, while advanced laboratory methods have promise for therapeutic planning purposes, monitoring response with repeated in vitro testing via biopsy is often impractical or impossible. In vitro material can be difficult to obtain and cancer adaptability and evolution over time can limit the utility of these studies. For example, histopathologic determination of the proportion of viable to nonviable cells after treatment correlates well with patient survival, but can only be applied to neoadjuvant therapies and cannot be repeated over time [5–7].

Particularly as targeted therapies have become standard components of several cancer regimens, the ability to monitor the effect of these molecules clinically through noninvasive imaging techniques has become of great interest. Determination of nonresponders early in the therapeutic course through imaging critical molecular processes within cancer can lead to better treatment efficacy and fewer drug-related complications. Effective post-treatment evaluations can also give clinicians a means of targeting patients that need close follow-up. As it has become recognized that early determination of treatment efficacy is both critical for patient care and can be difficult or impossible to ascertain with current imaging methods, the evaluation of molecular biomarkers, noninvasively, at several points throughout the therapeutic course has served as the driving rationale for the development for many molecular imaging methods.

Several approaches for uncovering the cell-level effects of cancer therapy through molecular imaging have been developed and show promise as effective tools for tailoring and monitoring the therapeutic course. In this section we begin by briefly describing the current methods for monitoring clinical cancer response and then provide an overview of the most well-studied emerging molecular imaging techniques being developed for clinical cancer management.

Anatomic determination of therapeutic response

The evaluation of primary and metastatic tumor volumes, locations, and lymph node involvement via diagnostic imaging (along with pathology, when available) serves as the foundation for patient staging, treatment planning, and prognostic stratification. Anatomic measures of solid tumors have been the standard means by which therapy effectiveness is judged for many decades. Nearly all early phase trials for cancer therapeutics use reductions in total tumor bulk as a proxy for tumor progression or patient survival and are critical for managing trial completion time and cost.

However, there are several fundamental and practical limitations with using purely anatomic measures as a survival proxy. Firstly, some cancers are known to be not suitable for dimensional evaluation based on diameter, such as mesothelioma. While changes in tumor size are often correlated with patient survival times, this is not always true (melanoma and renal cell carcinoma being notable exceptions) [8]. Emerging agents are often not cytocidal (cell killing) but are either slowing or blocking tumor growth; thus, RECIST criteria are not helpful for (early) response assessment [9]. A phase III study evaluating erlotinib in non-small cell lung cancer patients demonstrated a median overall survival increase in 43% despite an anatomic response rate of less than 10% [10]. Further, anatomic response to cancer therapeutics can be delayed well beyond therapeutic inception, requiring additional scans weeks after treatment. Finally, even with improved RECIST guidelines in place, their application can be difficult as it is often clinically difficult to delineate between post-treatment scar tissue and residual tumor mass. Variability in tumor burden assessment can vary as much as 100% between different investigators [11].

Physiologic/tumor perfusion imaging

Imaging the effect of therapy on physiologic measures, namely, determining tumor perfusion through dynamic changes in contrast enhancement, has become an attractive adjunct to objective anatomic response measures. Use of contrast agents to provide enhancement of tumor tissues has become a very common technique in the application of static CT and MRI in tumor imaging, often providing clinically improved detection and characterization of cancer lesions [12–15]. The improved enhancement achieved through intravascular contrast administration is based on differences in the rate of contrast movement from intravascular to extracellular extravascular space between normal and tumor tissues, and its retention within these tissues. Accordingly, changes in contrast enhancement over time can provide additional information about tumor perfusion and serve as a proxy for tumor microvessel density (MVD), a known prognostic factor in many cancer types [16–18]. Actual pathologic assessment of MVD is invasive, may not be repeatable, and depends on where the sample was taken within the tumor (vessel density is highest at the periphery) [19]. Critically, in vivo measures of tumor perfusion may also predict therapeutic response to agents that target and disrupt tumor microvasculature.

Static physiologic imaging

The change in contrast before and after the administration of iodinated contrast media is a simple method for approximating tumor perfusion. This change is commonly the difference between mean tumor signal before and after contrast administration (the “tumor perfusion score”) or the percentage of tumor above a certain signal threshold (the enhancing fraction, or “E_F”). The enhancing fraction in particular has been investigated as an easily measured biomarker for predicting therapeutic response, given that it requires only one pretreatment contrast scan. A recent study using E_F to predict clinical outcome of first-line therapy in patients with epithelial ovarian carcinoma found that E_F from a single pretreatment scan correlated with radiologic and CA125 response, as well as time to progression [20]. Similar findings have been demonstrated in patients with gliomas and breast cancer liver metastases [21,22]. However, some studies show conflicting results: in one study of cervical cancer, high levels of tumor perfusion predicted a better clinical response to radiotherapeutic intervention, while other studies have shown opposite results [23,24]. Currently E_F thresholds are determined post hoc, and further prospective analyses are needed to confirm these preliminary findings and potentially to establish tumor-specific cutoff values.

Dynamic contrast enhancement (DCE) imaging

The majority of clinical scans are acquired at a single point of time, providing an anatomic snapshot. However, repeated imaging of tumor enhancement during and after contrast administration can allow for a dynamic, quantitative assessment of perfusion. One measure commonly acquired through this method is the initial area under the contrast agent concentration curve (IAUC), which can be an effective indicator for tumor blood flow and vascular permeability [25]. Alternatively, with the application of kinetic models, quantitative measures of essential pharmacokinetic parameters such as vascular permeability, blood flow, vascular surface area, and interstitial pressure can be assessed [26,27]. The rate of volume transfer between plasma and extracellular extravascular space (K^{trans}) is often used as a composite of these quantitative parameters and is a commonly used as a measure of tumor vessel permeability (Fig. 1) [28].

DCE CT is simple to perform, as CT is widely available, quick, and provides a high degree of spatial resolution; however, because DCE requires repeated measures, the high level of ionizing radiation in repeated CT scans limits its wide applicability [29]. With the development of technologies that have allowed faster image acquisition via MR, the rate of image acquisition that is necessary for assessing the pharmacokinetics of gadolinium in tumor vasculature has become possible. Several studies have demonstrated the viability of DCE for use in treatment response predictions [30–33]. DCE MR has been shown to be effective in detecting response to therapy with PTK787/ZK 222584 [a vascular endothelial growth factor (VEGF) inhibitor] as early as 2 days after therapy, by measuring reductions in post-therapeutic contrast enhancement and permeability parameters [34]. Similar findings were detailed in DCE MR images taken of patients being treated with AG-013,736 [an inhibitor of the VEGF, platelet-derived growth factor (PDGF), and c-Kit receptor tyrosine kinases] and SU5416 (a selective inhibitor of VEGFR-2 tyrosine kinase) [35,36]. While DCE MR is a promising method both for the evaluation of novel antiangiogenic drugs and evaluating patients' clinical response, lack of standardization across imaging analysis and acquisition has made study reproducibility a challenge. Assumptions used to model pharmacokinetic parameters, vascular contrast concentration calculation versus direct measurement, and contrast dosing can all vary between studies [32,37].

Molecular imaging methods

Beyond macroscopic imaging of tumor anatomy and perfusion, molecular imaging has the capacity to characterize biologic processes at the cellular and subcellular level, noninvasively, within living organisms. While molecular imaging is still a developing field, a wide variety of techniques are emerging, all of which are designed with the purpose of translating fundamental physiologic and disease processes into a signal discernable through imaging contrast. Predicting response to cancer therapy has been a central motivation for the development of this technology; this is generally accomplished by pairing a method of generating a disease-specific signal with a means of transducing that signal into one that can be readily detected by the desired imaging modality. The application of molecular imaging in cancer therapy is reliant on the direct measurement of one or more of the underlying biomolecular hallmarks of cancer cells that is altered in neoplastic transformation (Fig. 2) [38].

A cancer-specific signal can be generated either by designing reporter molecules which will concentrate in areas of disease (through, for example, specific interactions with stationary tumor biomarkers) or through "activation" of the reporter in environments that exhibit pathophysiologic conditions (such as a high pH). Using molecular imaging to detect sustained growth, antiapoptotic signals, sustained angiogenesis, or other cancer properties

can both lead to easier differentiation from normal tissue and can relate how effectively a therapy is modulating these markers.

Molecular imaging modalities

Depending on the method by which molecular tumor specificity is generated, differing imaging modalities can be employed to translate that specificity into readily interpretable images. While many imaging modalities are being tested and employed for molecular imaging in research [39–42], radionuclide imaging is currently the most commonly utilized modality for leveraging molecular imaging in identifying responses to treatment in cancer. Nuclear medicine relies on the measurement of short-lived radioisotopes tracers, which, in the case of molecular imaging, can be incorporated into natural biomolecules that can detect physiologic processes in the body in ways not possible by any other imaging technique. Further, isotopic imaging is highly sensitive and is a useful modality for establishing target specificity.

Metabolic imaging

Metabolic imaging through the application of the glucose analog ^{18}F-fluorodeoxyglucose (FDG) using PET is the first and currently only molecular imaging method with wide application in clinical oncology. FDG PET has become standard of care at several phases of the diagnostic work-up for oncology patients and is an essential tool for differentiating between malignant and benign lesions, for gauging response to radio- and chemotherapies, and for identifying tumor recurrence and potential metastatic lesions. Increasingly FDG PET has been used for post-therapeutic evaluation therapy in conjunction with anatomic imaging and has, in several instances, been shown to be superior to anatomic-based response categorization in determining outcomes.

The now near universal adoption of FDG PET is in part a response to its ability to quantify cellular metabolism in vivo at multiple points throughout the treatment course. Post-therapeutic decreases in metabolic activity, as measured by FDG PET, have correlated well with overall survival, even in instances where anatomic evaluation via CT demonstrates residual tumor tissue. This has been recognized clinically, where an estimated 19% of PET scans performed in the USA are for response monitoring [43].

FDG PET imaging of therapeutic response—The use of FDG PET to measure the progress of cancer therapy in advance of anatomic changes was demonstrated in 1993 by Wahl et al. in patients receiving chemotherapeutics for breast cancer [44]. This finding has subsequently been demonstrated in several additional solid tumor types and has been the subject of several reviews [45–47]. There is, for instance, mounting evidence which demonstrates that FDG PET response monitoring in several cancer types such as colorectal cancer and gastrointestinal stromal tumor (GIST) is a significant predictor of outcome beyond objective anatomic response [48].

In solid tumors, studies have largely focused primarily on the use of FDG PET in identifying therapeutic nonresponders, given that these tumors frequently have poor response to the current therapeutic armamentarium. Within non-small cell lung cancer (NSCLC), the emergence of neoadjuvant therapies have expanded therapeutic options for patients, but have made treatment monitoring ever more critical (Fig. 3) [49,50]. One trial found that in NSCLC patients there was a 60% discordance between therapeutic responders by CT versus PET and that of all other clinical and anatomic imaging criteria, only PET significantly correlated with survival [51]. An interesting finding in a recent prospective multicenter trial for primary breast cancer showed that a metabolic response to a single cycle of treatment, regardless of the type of chemotherapy, could predict patient outcomes [52]. Another

significant result from this trial was the demonstration that low pretreatment PET activity showed poor response to primary chemotherapy overall, a finding which could imply alternative treatments (with immediate surgical resection or hormonal modulation) would be useful for these patients [52,53].

FDG PET-based therapeutic modification—The establishment of FDG PET's significance for response monitoring in the literature has led to a great deal of interest in codifying the use of FDG PET for modification of therapy based on early metabolic response; however, large randomized clinical trials are necessary to bring this to fruition. A single center study was conducted in esophageal cancer patients in which repeat FDG PET imaging after 2 weeks of therapy was used to identify chemotherapeutic nonresponders, who then discontinued therapy and had immediate surgical resection; this trial showed promising survival data, and a phase III trial is planned [54]. Of note, a recent multicenter trial was also conducted to identify nonresponders in locally advanced esophageal cancer to shorten preoperative therapy; however, PET did not yield enough clinical accuracy to justify early treatment withdrawal [55].

FDG PET response criteria and limitations—The literature around lymphoma has consistently demonstrated superior outcome predictions than those that are generated with CT imaging, which has recently led to revisions in the International Working Group's response criteria which rely heavily on PET imaging [56]. However, despite analogous findings in solid tumors, recommendations for the application of FDG PET in measuring therapeutic response in specific clinical scenarios have not yet been established. This is largely due to the differences in study methodology, PET acquisition timing, histopathologic interpretation and/or clinical endpoint, as well as a lack of common definitions for therapeutic response [48,53,57]. These discrepancies have resulted in a lack of consistency across studies that has prevented a consensus determination on what construes the change of FDG uptake, particularly across differing cancer types [47]. Standard interpretation of PET scans with "mild" or borderline FDG uptake changes after therapy are particularly difficult and has different prognostic significance for differing tumors. Additional study variation can be attributed to differences in the kind of measures used in PET: while the European Organization for Research and Treatment of Cancer (EORTC) recommended using body surface area to standardize FDG uptake as measured by the standard uptake value (SUV) in 1999, several other measures are in use, including body weight and the metabolic rate of glucose (MRGlu) [58].

Efforts are ongoing to establish guidelines for PET therapeutic response. The 1999 EORTC proposal developed a framework on which to build standards for FDG PET-defined response, defining complete response as indistinguishable from surrounding normal tissue and partial response as a 15–25% reduction in pretreatment SUV after a single therapeutic cycle, or greater than 25% after more than one cycle. Progressive disease would be defined as an increase in the SUV from the baseline scan by 25% or more, or the emergence of new metastatic sites, and stable disease is declared if conditions for any of the other disease determinations are not met. Additionally RECIST 1.1 guidelines acknowledge that FDG PET is an important adjunct to CT in the determination of progressive disease and disease recurrence, but does not incorporate PET imaging into any of the core measurements of disease burden [59]. There are over 30 methods for quantifying FDG PET response currently used in practice, and work on developing an established standard is ongoing [57].

Efforts to provide standard measures for therapeutic response notwithstanding, FDG PET has fundamental limitations as well: it is confounded by factors that alter non-neoplastic tissue metabolism, such as hypoxia, inflammation, and serum glucose level. In some tissues where glucose uptake is constitutively high, as is the case with brain gray matter, PET

sensitivity is significantly reduced [60]. PET response in recurrent tumors is less likely to predict effective clinical response, as many of these recurrent tumors have lower metabolic rates and are in the setting of inflammatory scar tissue [61]. Perhaps most critically, FDG PET imaging can only inform clinicians about one dimension of cancer pathophysiology. Other in vivo measurements of cellular properties beyond FDG PET are likely to yield critical information for oncology treatment as well.

Cellular proliferation imaging (FLT PET)

Along with metabolism, cellular proliferation was among the first biomarkers of interest targeted by molecular imaging in clinical oncology, given the diagnostic and prognostic significance of this characteristic of cancer. More specifically, the process of DNA synthesis that coincides with cellular reproduction has been a clear area of focus and a commonly targeted molecular process for developing repeatable in vivo measurements of proliferation. The first efforts to accomplish this goal attempted to translate an analogous in vitro immunohistochemical process that is based on the application of labeled thymidine nucleoside precursors to recently excised tumors for measuring the proportion of tumor cells actively synthesizing DNA [62]. Measurement of labeled thymidine incorporation is still the gold standard for proliferation-based prediction of prognosis, even though clinically it has been largely replaced by assays measuring Ki-67/MIB-1 (proteins that are expressed only in actively dividing cells) because of the test's relative simplicity and reliability.

Accordingly, the most studied class of tracers of proliferation studies to date have been the thymidine analogs, which have been studied for in vivo imaging of proliferation for several decades [63]. The first such efforts yielded [^{11}C-methyl]TdR, and its predecessor 2-^{11}C-TdR, both of which showed promise for proliferation monitoring but were too difficult to implement clinically, because of their short half-lives and their high rate of catabolism, which required sophisticated kinetic analyses [64]. Among the thymidine analogs, 3′-deoxy-3′-[^{18}F]fluorothymidine (FLT) is now the most commonly used and studied, largely because of its suitably long half-life and resistance to in vivo degradation [65].

FLT imaging validation and preclinical studies—Originally designed to be an antiretroviral or antineoplastic drug meant to terminate DNA synthesis, FLT creates imaging contrast by concentrating in replicating cells through its active transportation across the cellular membrane and subsequent cellular trapping through phosphorylation by thymidine kinase 1 (TK1). TK1 is an essential enzyme and rate-limiting step in the exogenous (salvage) pathway for thymidine generation in DNA synthesis; it is nearly absent in quiescent cells, but is upregulated in proliferating cells [66].

Validation of FLT PET, typically measured against Ki-67 cellular proliferation assays, has met with mixed results, depending on the cancer type. In breast and in brain cancer FLT activity was shown to be correlated with in vitro proliferation measurements, and comparisons of FDG versus FLT imaging for proliferation in lung tumors have generally favored FLT [67,68]. However, correlation with FLT PET activity and proliferation markers was not established in esophageal cancers, demonstrating variability of FLT based on cancer type [69–71]. FLT studies appear to be generally repeatable: de Langen et al. established that semiquantitative FLT imaging techniques were as accurate as more complex kinetic studies and that changes of 20–25% or more can be attributed to treatment-related changes [72].

Several animal studies have shown early and pronounced reductions in FLT uptake after chemotherapy as compared with FDG PET. Some studies have demonstrated FLT PET response to radiotherapy within 24 h of treatment [73–76]. In one example, Pan et al. showed that irradiated mammary MCaK tumors showed changes in FLT PET activity 24 h

after a 5-Gy dose using both kinetic and semiquantitative methods [77]. FLT PET response appears to be therapy dependent; however, one recent study using a murine follicular lymphoma model showed significant FLT activity reduction after chemotherapy, but not after administration of immunotherapeutic agents or radioimmunotherapy, even in the presence of demonstrated changes in proliferation by histology [76]. This implies that post-therapeutic uptake of FLT is dependent on a broader set of cellular changes than those responsible for proliferation.

Clinical FLT studies—FLT has provided some limited utility in cancer detection and staging. For example, FLT has shown some promise as a method for increasing specificity for neoplasm in patients with solitary lung nodules [78]. However, studies thus far have suggested a limited role in staging, as FDG generally provides better cancer to normal tissue contrast than FLT. A potential exception is in brain tissue, where FDG PET has poorer tumor contrast due to the high background metabolic rate of gray tissues. FLT PET has shown promise in detecting gliomas and in one study has been shown superior to FDG imaging in differentiating low- and high-grade brain tumors from non-neoplastic processes [69,79]. Thus, FLT PET may serve as an adjunct to FDG for cancer screening and detection in some limited indications.

Human trials to validate FLT therapeutic response have been limited, but these preliminary studies have shown some promise. Two small studies of breast cancer patients demonstrated correlation between FLT activity reduction and therapeutic response, one which showed a significant difference in SUV_{max} at 1 week between patients with stable disease versus clinical response [80]. FLT PET may have additional utility for characterizing emerging therapies with heterogeneous response profiles. For example, Sohn et al. demonstrated that therapeutic response by conventional imaging in patients with adenocarcinoma of the lung to the EGFR inhibitor gefitinib could be effectively predicted at 1 week after the start of therapy using FLT imaging (Fig. 4) [81]. Using changes in SUV_{max}, the investigators were able to predict objective anatomic response with positive and negative predictive values of 92.9%. While overall survival between groups was not significant, and the SUV_{max} threshold was determined post hoc, this study demonstrates promise for FLT as a potentially useful tracer for imaging therapeutic response.

FLT PET limitations and future directions—FLT PET imaging has significant limitations: FLT is highly retained in bone marrow as well as in the liver, where it undergoes extensive glucuronidation, leading to high background enhancement in these tissues and reducing the potential utilization of FLT near these organs [82]. Proliferation of lymphocytes within lymphatic tissues can also lead to false positives by FLT [83]. Beyond this, it is clear from these preliminary studies that the relationship between proliferation and FLT PET enhancement is not a simple one, and further study is needed. Uptake is generally lower than FDG, and further kinetic studies are necessary to ensure FLT stays within the cells in question. FLT uptake is dependent upon TK1 activity through activation of the salvage pathway, which does not correlate with proliferation in all tumor types; in some cancers, the de novo pathway appears to be dominant, which may explain the variability of post-therapeutic response between cancer types [71,84]. Additionally, different therapeutics may have unexpected effects on key components of this pathway, which may confound the interpretation of post-therapeutic changes [85]. Therefore, it remains to be seen whether FLT can become an effective predictor of overall survival.

Angiogenesis imaging

Angiogenesis is a highly regulated process in normal physiology; however, cancer cells often promote local angiogenesis to support tumor growth. Tumors are generally limited to a

diameter of 2–3 mm without additional blood supply, so neoplastic lesions are generally not life-threatening until the milieu of pro- and antiangiogenic factors shifts in the favor of vessel development [86,87]. Markers of increased angiogenesis have been recognized as effective targets for therapeutics, as well as a promising, novel means of cancer imaging [88,89]. Following the success of the anti-VEGF antibody therapeutic bevacizumab as a first-line cancer therapeutic, interest in development of angiogenic pathway modulators has grown substantially.

Antiangiogenic agents are generally cytostatic and do not necessarily cause large reductions in tumor volume on a short timescale even when they are effective, which reduces the utility of anatomic measures in monitoring response to these agents. Physiologic imaging methods of measuring tumor perfusion discussed previously, like DCE MR, have some utility for assessing therapeutic response, but cannot reflect the more immediate molecular level a therapeutic may have. FDG PET studies of tumors treated with antiangiogenic therapies often result in a paradoxical increase in activity, which makes interpretation of post-therapeutic studies using current techniques difficult [90]. Several angiogenesis imaging tracers are currently in clinical and preclinical testing and hold promise for future application in therapeutic response monitoring.

RGD imaging—Integrins are heterodimeric transmembrane glycoproteins that function in a wide variety of cell-extracellular matrix and cell-cell interactions [91,92]. This class of proteins is essential in cellular migration, metastasis, and in the development of new vessels. The various integrin dimers can combine to create at least 24 integrin types, though integrin $\alpha_v\beta_3$ has been the most thoroughly studied to date [93]. A common property to many integrins, including $\alpha_v\beta_3$, is their interaction with the arginine-glycine-aspartic acid (RGD) sequence found in extracellular matrix proteins like vitronectin, fibrinogen, thrombospondin, and fibronectin [94]. Expression of $\alpha_v\beta_3$ and the production of proteases such as matrix metalloproteinases (MMPs) allow the migration of endothelial cells through the interstitial matrix during vessel formation [95,96]. In addition, $\alpha_v\beta_3$ is expressed on the surface of a variety of tumor cell types, which aids in tumor migration and metastatic spread [97,98].

Haubner et al. developed the first radiolabeled RGD peptide markers for use in vivo, which showed good tumor affinity (particularly for the M21 melanoma tumor model), but had early clearance and high uptake in the liver [99]. Since that time, several advancements, such as conjugation with hydrophilic amino acids, sugar moieties, and polyethylene glycol (PEG), have led to much improved pharmacokinetic profiles [100,101]. Based on refinements through affinity studies several RDG peptide alterations have been made, and now both linear and cyclic pentapeptide forms of RGD are frequently used [102,103]. A variety of radiohalogenated or radiometalated RGD conjugate types have been developed using various chelator methods, like diethylenetriaminepentaacetic acid (DTPA), 1,4,7,10-tetraazacyclododecane-*N*-*N*′-*N*″-*N*‴-tetraacetic acid (DOTA), and others [104–106].

Initial clinical studies of RDG tracers have shown good tumor to background activity, rapid renal clearance, and dosing that correspond closely with that of FDG PET [107]. Histologic studies have confirmed that RGD uptake correlates closely with tumor $\alpha_v\beta_3$ integrin expression [108]. Integrin $\alpha_v\beta_3$ is predominantly expressed in endothelial cells, so RGD tracers correlate with microvascular density as well [109]. Significantly, in a comparative study in patients with non-small cell lung cancer, there appears to be no correlation between FDG PET and ^{18}F-galacto-RGD tumor activity across several tumor types, so each technique likely provides unique, independent information on molecular tumor processes (Fig. 5) [110].

Physiologic RGD interactions are thought to be based on multivalent interactions with clusters of integrin membrane proteins. To identify tumors more effectively in areas of high physiologic integrin expression, such as the liver, spleen, and intestine, advancements in tumor specificity have been achieved by using multiple RGD peptides per tracer isotope. In mice with SK-RC-52 renal cell carcinoma xenografts, monomeric, dimeric, and tetrameric cyclic RGD tracers conjugated with DOTA and radiolabeled with ^{111}In showed that tumor uptake of the tetramer exceeded that of both the dimer and the monomer [111]. Further, in vivo microPET imaging demonstrated higher uptake and retention using ^{64}Cu-DOTA-RGD octamer in U87MG human glioblastoma tumor grafts as compared with tetramer versions [112]. Using PEG_4 linkers to introduce distance between RGD motifs has also been shown to increase tracer affinity [113]. Additionally, binding ligands for $\alpha_5\beta_1$, an integrin that has low baseline endothelial expression but is highly expressed during neovascularization, are currently under development [114]. There are not yet significant data on the use of RGD imaging for measuring therapeutic response, but RGD imaging is likely to have application in monitoring antiangiogenic agents.

VEGF imaging—VEGF-A (commonly referred to as VEGF) is a potent mitogen and key regulator of neovascularization in development, somatic growth, and neoplasm. Alternative mRNA splicing results in at least seven isoforms of VEGF with varying solubility characteristics and receptor binding affinities, and can be excreted into the extracellular matrix or be bound to cell surface proteoglycans [115–117]. There are two VEGF receptor tyrosine kinases types, VEGFR-1 and VEGFR-2, which are expressed primarily on endothelial cells. VEGFR-1 expression varies with the stage of development, cell types, and on physiologic state, while VEGFR-2 is believed to be the key transducer for angiogenic and mitogenic properties [118]. An elevated level of VEGF is a known poor prognostic sign in cancer, correlating with increased metastatic invasion [119]. As other agents emerge to modulate the VEGF pathway, noninvasive imaging agents have emerged to provide molecular tumor characterization for optimizing these therapies.

VEGF imaging has been accomplished largely by using radiolabeled antibodies; the first imaging of VEGF expression was performed utilizing radiolabeled bevacizumab, in mice with SKOV-3 ovarian xenografts [120]. VG76e, an IgG1 antibody targeted against VEGF, showed high tumor to background contrast, but the antibody showed poor immunoreactivity, limiting the tracer's potential use as an imaging agent. In a phase I trial of HuMV833 humanized anti-VEGF antibodies, patients with solid tumors were imaged using radiolabeled HuMV833 after treatment with the antibody. Distribution and clearance were found to be heterogeneous both between patients and individual tumors [121]. ^{111}In-labeled bevacizumab has been used to image VEGF in colorectal cancer patients with liver metastases. In this study, 9 of 12 patients with metastatic lesions were detected with labeled bevacizumab; however, surprisingly no correlation was found between the level of antibody accumulation and expression of VEGF in postresection analysis [122]. The apparent difficulties in VEGF imaging are likely to be related to the dynamic nature of VEGF's soluble forms.

An alternative approach has been to image VEGFR expression using radiolabeled soluble forms of VEGF, like $VEGF_{121}$. ^{64}Cu-DOTA-$VEGF_{121}$ demonstrated prominent uptake in small U87MG grafts, which are highly vascularized, but significantly lower and sporadic uptake in large U87MG tumors, which have less prominent vascularization [123]. A follow-up study demonstrated VEGFR-2 expression was increased in a narrow window of tumor sizes [124]. The finding that VEGFR expression is modulated during the progression of a single tumor may imply repeated VEGFR-targeted studies may be useful for guiding antiangiogenic therapies [123]. An imaging study of a VEGFR-specific toxin, $VEGF_{121}$/rGel (composed of $VEGF_{121}$ linked to the plant toxin gelonin), demonstrated high contrast

in glioblastoma tumor grafts [125]. Histology confirmed microvascular damage in the tumors after four treatments of $VEGF_{121}$/rGel and shows the promise for VEGFR targeting for both imaging and therapeutic interventions.

MMP imaging—MMPs are a family of extracellular proteins which enzymatically disrupt the structural components of the extracellular matrix and basement membranes. The over 20 identified MMPs have been observed to play various roles in angiogenesis, development, wound healing, and the generation and release of growth factors, cytokines, chemokines, and proteinase inhibitors [126–128]. While many MMPs are expressed by malignant cells to promote angiogenesis and metastatic dissemination, MMP-2 and MMP-9 are most consistently present across cancer types [129–131].

Koivunen et al. discovered a cyclic peptide known as CTT through phage display techniques that inhibit MMP-2 and MMP-9 activity that prevents tumor growth and metastasis [132]. ^{111}In-radiolabeled CTT was used to measure MPP-2 and MMP-9 expression levels and showed a significant correlation between signal and both normal and tumor tissue MPP activity [133]. However, CTT imaging is currently limited by relatively poor tumor uptake and peptide stability [134]. Another approach to imaging MMP activity has been through labeling small molecule MMP inhibitors, such as CGS 25966 and CGS 27023A, which deactivate MMP by chelating the zinc ion of the active site [135,136]. ^{11}C and ^{18}F versions of these and other MMP inhibitors have been developed but have suffered from poor tumor contrast and nonspecific activity in preclinical trials [137,138]. While additional MMP tracers with different isotopes have been developed as well, significant improvements in MPP will be necessary before tracers could be used clinically.

Other angiogenesis imaging methods—Several additional angiogenesis biomarkers have been identified that may have efficacy for angiogenesis imaging in the future. For instance, fibronectin is a large glycoprotein present in plasma and in extracellular matrix. However, fibronectin attains a 91 amino acid sequence known as the “extra domain B” through alternative splicing in the setting of angiogenesis and in the presence of a variety of solid tumors [139]. Several antibodies and antibody fragments have been developed to target extra domain B [139,140]. One such antibody, L19, was labeled with ^{123}I and was able to selectively identify actively growing (versus quiescent) colorectal and lung tumor lesions in patients [141].

Similar to fibronectin, tenascin is an extracellular protein that expresses extra domain C, which is present in astrocytoma vasculature, as well as in the majority of lung cancers [142]. A human antibody fragment with high affinity to extra domain C containing tenascin named G11 has been developed, which showed good contrast in an orthotopic rat glioma model [143]. Additionally, several other angiogenesis biomarkers, including Tie receptors and CD276, are also potential targets for angiogenesis imaging [144,145].

Hypoxia imaging

Hypoxia is a well-known poor prognostic factor in patients with a variety of primary tumor types [146–148]. Hypoxic tumor cells have increased radio- and chemotherapeutic resistance as well as increased metastatic activity, resulting in an increased failure of local control [149,150]. The importance of hypoxia in tumor pathophysiology and its prognostic relevance makes a standard diagnostic methodology for its measurement desirable, particularly in planning radiation therapy [151]. The current gold standard method, placement of oxygen-sensing electrodes, is invasive and suffers from significant intraoperative variability [147]. Several noninvasive MR techniques have been developed, including measurement of oxygen tension by detecting levels of paramagnetic

deoxyhemoglobin or by using injections of free radical contrast agents with subsequent measurement of paramagnetic electron resonance [152,153]. However, flow heterogeneity and other factors limit the reliability of functional MR techniques and have further promoted the development of novel hypoxia-specific radiotracers [152]. Early studies of emerging hypoxia-sensing tracers, like ^{18}F-fluoromisonidazole (^{18}F-FMISO) and $^{60/61/62/64}$Cu-labeled diacetyl-bis(N^4-methylthiosemicarbazone) ($^{60/61/62/64}$Cu-ATSM), two of the most successful such imaging agents, have shown promise as potential adjuncts to standard cancer imaging techniques.

FMISO imaging—FMISO is the most extensively studied tracer in the nitroimidazole class of agents, which convert to a prolonged reduced state in hypoxic tissues and ultimately bind with intracellular macromolecules causing retention within viable hypoxic cells [154]. Several studies have demonstrated positive ^{18}F-FMISO uptake (generally defined as a tissue to blood ratio of greater than 1.2 at 2 h post-administration) negatively correlates with overall survival in patients with head and neck cancer [155,156]. Rischin et al. found that in patients with stage III and IV head and neck squamous cell carcinoma (SCC) demonstrating anoxia by FMISO had significantly decreased locoregional failure (LRF) rates when using a tirapazamine-containing chemoradiotherapy (a prodrug that converts to active form in low oxygen environments) as compared to the standard platinum/fluorouracil-based therapy [157]. While protocols for treatment in the setting of hypoxia have not been established, this study demonstrates the potential for such an approach. However, preliminary studies have shown mixed results in different tumor types. In a study of 22 patients with glioblastoma multiforme tumors, hypoxia as measured by ^{18}F-FMISO activity was correlated with decreased time to progression and survival in patients receiving radiotherapy (Fig. 6) [158]. However, no ^{18}F-FMISO activity correlation was found in patients with non-small cell lung cancers [159].

While FMISO is lypophilic and readily crosses cellular membranes, it suffers from poor tissue penetration, resulting in low contrast between hypoxic and normal tissues. Further, FMISO has a slow cellular washout rate, requiring image acquisition to take place 2 h after administration to allow normal tissue clearance, by which time ^{18}F will have decayed by greater than one half-life ($T_{1/2}$=109.7 min). These limitations have largely restricted the use of ^{18}F-FMISO in clinical practice [160]. Several alternatives have emerged: ^{18}F-fluoroazomycin arabinoside (FAZA), for example, is cleared from background tissues more quickly and thus results in higher tumor to background ratios [161]. In patients with head and neck cancers, FAZA showed slightly higher tumor to background ratios (hypoxia was defined as a ratio greater than 1.5), and significant inter-patient and inter-tumor heterogeneity was apparent [148]. Similar findings were demonstrated in the 2-nitroimidazole agent ^{18}F-2-(2-nitro-^{1}H-imidazol-1-yl)-*N*-(2,2,3,3-pentafluoropropyl)-acetamide (EF5), which has shown both improved kinetics and the ability to identify both soft tissue sarcomas and brain tumors with high metastatic potential, but the key problem for EF5 is poor yield of radiosynthesis [162,163]. Similar agents are emerging, like ^{18}F-1-(2-fluoro-1-[hydroxymethyl]ethoxy) methyl-2-nitroimidazole (FRP170) and other nitroimidazole tracers, which boast improved biodistribution properties. However, many have not yet been tested for clinical utility [164,165].

Cu-ATSM imaging—Cu-ATSM is the most common and well studied of the dithiosemicarbazone-based hypoxia imaging agents. Similar to FMISO, Cu-ATSM undergoes reduction and is trapped within hypoxic cells; however, Cu-ATSM is reduced in states of more mild tissue hypoxia, with threefold greater retention in tissues with partial pressures of oxygen between 0.1 and 0.5% [166]. Various isotope candidates have been considered in conjunction with Cu-ATSM, including ^{60}Cu ($T_{1/2}$=23.7 min), ^{61}Cu ($T_{1/2}$= 3.35 h), ^{62}Cu ($T_{1/2}$=9.74 min), and ^{64}Cu ($T_{1/2}$=12.7 h). Cu isotopic labeling provides greater

flexibility with timing than ^{18}F, and Cu-ATSM exhibits improved pharmacokinetics with quicker normal tissue clearance than FMISO, allowing imaging acquisition within an hour and greater resultant tumor to background ratios.

Cu-ATSM was originally used successfully for delineating ischemic myocardial tissue in animal studies [167,168]. A preliminary human trial showed increased myocardial uptake in one patient with unstable angina [169]. Cu-ATSM was evaluated in lung cancer patients, which demonstrated a strong tumor contrast with high tumor to background ratios (mean of 3.00 and max. of 9.33) [170]. Further studies evaluating Cu-ATSM in cervical and rectal cancer have been encouraging as well [171–173]. Dietz et al. demonstrated that tumor tissue with increased Cu-ATSM activity (ratios greater than 2.6) had poorer overall and progression-free survival. The study also demonstrated that Cu-ATSM activity was independent of FDG PET activity [171]. Similar results were found in patients with cancer of the uterine cervix, which also compared ^{60}Cu-ATSM and ^{64}Cu-ATSM image quality and found the much longer lived ^{64}Cu-ATSM to be superior. This finding may pave the way for the large-scale production needed for multicenter validation trials [173]. A recent study demonstrated that small cell carcinoma showed high Cu-ATSM and low FDG activity at the periphery of the tumors but low Cu-ATSM and high FDG uptake at the center [174]. This pattern was not present in lung adenocarcinoma, indicating that combined Cu-ATSM and FDG PET studies could be a means for future diagnostic differentiation. However, Cu-ATSM may not be an effective hypoxia marker in all cancer types: in a study validating Cu-ATSM activity in animal models of various tumor types with histopathologic evaluation, correlation could not be established in fibrosarcoma tumors [175].

Apoptosis imaging

Apoptosis, or programmed cell death, is a highly regulated cellular process by which cells die in both healthy and disease states [176]. As opposed to necrosis, which is disordered cellular death generally arising from acute cellular damage, apoptosis is a multistep process by which cellular components are degraded and packaged into apoptotic bodies for ordered phagocytosis [177]. DNA damage, immune reactions, ischemic injury, as well as chemo- and radiotherapy all can lead to the activation of the apoptotic process. Additionally, apoptosis is the most common pathway for treatment-induced cancer cell elimination and lack of apoptosis can potentially be a sign of treatment failure. Therefore, apoptosis has been viewed as a potentially useful biomolecular process for treatment assessment through in vivo imaging [178,179].

Annexin V imaging—Phosphatidylethanolamine (PE) and phosphatidylserine (PS) are reliable apoptotic cellular surface signals that aid in cellular degradation and phagocytosis [177,180]. In nonapoptotic cells, aminophospholipid translocase has ATP-dependent action to keep PE and PS on the inner surface of the cellular phospholipid bilayer [181]. However, when apoptotic pathways are activated, PE and PS are expressed on the cell surface through Ca^{2+}-dependent deactivation of translocase and the activation of scramblase, which ultimately facilitates apoptosis of the cell [182]. Accordingly, PE and PS are common targets in apoptosis imaging. Annexin V, a human anticoagulant protein, selectively binds PS in a Ca^{2+}-dependent fashion and has been utilized in several capacities for labeling apoptotic cells [182,183].

Blankenberg et al. were the first to use annexin V for in vivo imaging using ^{99m}Tc labeling and demonstrated that murine lymphoma xenografts had higher activity 3–4 h after treatment with cyclophosphamide [184,185]. The first trial in a population of 15 patients with late stage small and non-small lung cancer, Hodgkin's and non-Hodgkin's lymphoma, and metastatic breast cancer showed potential correlation between post-treatment ^{99m}Tc-

labeled annexin V SPECT activity and treatment response at 3 months [186]. This study demonstrated potential for annexin V imaging, but the labeling chemistry employed resulted in relatively low synthetic yields and nonspecific excretion into the bile, confounding any potential application in the abdomen [187]. An improved labeling technique using the agent hydrazinonicotinamide (HYNIC) has become standard because of its much improved yield, ease of labeling, and lack of bile excretion; however, HYNIC labeling has the drawback of increased radioactive signal in the kidney, limiting its use for perirenal imaging [188–190].

Additional studies in treatment of both small and non-small cell lung cancer showed correlations with an increase in baseline annexin V imaging activity and objective tumor response after platinum-based chemotherapies [190,191]. Lung cancer patients showed that tumor response correlated significantly with increases in annexin V SPECT imaging 48 h after the first cisplatin injection [191]. Kartachova et al. recently performed a study of 38 patients with mixed primary head and neck tumors that outlined quantitative and a qualitative guidelines, respectively, based on maximal counts per pixel or visual assessments, which resulted in highly specific response predictions and low inter-operator variability in both cases (Fig. 7) [192]. Additional studies in head and neck cancer, lymphoma, and breast cancer have demonstrated similar outcomes [193–195]. In an effort to lower kidney activity and increase tumor contrast, several annexin V mutants have been developed which can chelate isotope radiolabels without linkage molecules. The most well known of these mutants is V117, which contains a six amino acid sequence at the N-terminal end of the protein which chelates ^{99m}Tc and has the benefit of much lower in vivo renal retention [196]. A similarly modified annexin mutant, V128, showed approximately twice the level of uptake as annexin tracers that had been modified for labeling, presumably because these tracers had fewer binding sites [197].

Other apoptosis imaging techniques—Several other targeting agents have been developed for targeting the PE- and PS-expressing apoptotic cells. The C2A domain from synaptotagmin I, a membrane trafficking protein, binds to PS and was labeled with ^{99m}Tc to image non-small cell lung tumor graft response to intravenous paclitaxel therapy. A positive correlation was seen between activity and histologic measures of apoptosis [198]. Similar exploratory studies have been performed with ^{99m}Tc-labeled duramycin, a low molecular weight and highly stabile 19 amino acid peptide sequence that binds PE, which have shown promising results [199]. As an alternative to imaging apoptosis by targeting PE or PS, isatin sulfonamide analogs image the internal pathway of apoptosis by targeting caspases, which are essential proteolytic enzymes in the intracellular apoptotic cellular degeneration process. One such analog, WC-II-89, demonstrated proof of concept in an animal model with chemically induced hepatocyte apoptosis [200]. However, most caspase-based approaches have suffered from low tumor contrast rates in other studies [201].

Recently, a new group of agents known as ApoSense tracers have been developed which are able to selectively enter apoptotic cells. These tracers are low molecular mass, amphipathic agents that anchor to cell membranes at their hydrophobic domain, while relying on the increased movement of molecules between the inner and the outer layers of the cellular membrane during apoptosis to “flip” inside of dying cells and to bind a yet unknown apoptotic biomarker. A member of this class of molecules, NST-732, has been developed both with ^{18}F isotopic and fluorescence imaging capabilities, which demonstrated high activity in irradiated lymphoma and ischemia-induced experimental apoptosis states [202]. Didansyl-L-cystine (DDC) is a similar molecule which has shown promise after initial treatment monitoring studies in melanoma tumor models after treatment with chemotherapeutics [203]. While these molecules have yet to be fully characterized, ^{18}F-labeled 5-fluoropentyl-2-methyl-malonic acid (^{18}F-ML-10), a similar ApoSense small

molecule designed specifically for radiolabeling, is currently undergoing early stage clinical trials.

Conclusions and perspectives

While anatomic assessment of tumor changes is still the standard for assessing therapeutic response, several emerging techniques, based on a spectrum of physiologic biomolecular changes, are emerging to alter this paradigm. The development of guidelines for measuring FDG PET response through multicenter trials is needed, but is only a first step: continued validation is required for tracers that go beyond FDG PET to measure the full extent of cancer cell physiology. A number of other metabolic tracers such as radiolabeled amino acids and choline have already entered clinical trials. The continued validation of novel tracers, whether small molecules, peptides, antibodies, or other methods, has largely taken place within the realm of isotopic imaging, because of the modality's high sensitivity and quantitative capabilities. Still greater exploration and validation with PET will be needed to ensure the relationship between target binding and PET signal quantification before translation of these tracers to humans can be accomplished.

However, the greatest potential for these novel tracers will be achieved through leveraging a multimodality approach which takes advantage of multiplexed imaging techniques to generate a comprehensive evaluation of tumor physiology. Development of a multimodal imaging method would yield tremendous clinical benefits, including improved lesion detection, patient stratification, treatment monitoring, dose optimization, and drug development. For these benefits to be effectively realized, additional targets must be identified, optimized reporter labeling methods must be established, pharmacokinetic/dynamic characteristics must be further tuned, and additional clinical studies must take place. While novel tracers have traditionally suffered from poor clinical translation because of a perceived low market potential relative to the costs of development, this has gradually changed as the potential for these tools has increasingly come to light through accelerated research interest. Molecular imaging advances at the preclinical level and new US Food and Drug Administration (FDA) procedures allowing faster transitions to first-in-human trials have been a boon to the translation of new molecular imaging techniques to the clinic. Nevertheless, a concerted, focused effort and the allocation of additional resources are likely needed to effectively translate molecular imaging techniques to the clinical environment.

Acknowledgments

This research was supported by the Intramural Research Program of the NIH, NIBIB.

References

1. Ross JS, Fletcher JA, Linette GP, Stec J, Clark E, Ayers M, et al. The Her-2/neu gene and protein in breast cancer 2003: biomarker and target of therapy. Oncologist 2003;8:307–325. [PubMed: 12897328]
2. Allegra CJ, Jessup JM, Somerfield MR, Hamilton SR, Hammond EH, Hayes DF, et al. American Society of Clinical Oncology provisional clinical opinion: testing for KRAS gene mutations in patients with metastatic colorectal carcinoma to predict response to anti-epidermal growth factor receptor monoclonal antibody therapy. J Clin Oncol 2009;27:2091–2096. [PubMed: 19188670]
3. Pao W, Miller VA. Epidermal growth factor receptor mutations, small-molecule kinase inhibitors, and non-small-cell lung cancer: current knowledge and future directions. J Clin Oncol 2005;23:2556–2568. [PubMed: 15767641]
4. Vogel CL, Cobleigh MA, Tripathy D, Gutheil JC, Harris LN, Fehrenbacher L, et al. Efficacy and safety of trastuzumab as a single agent in first-line treatment of HER2-overexpressing metastatic breast cancer. J Clin Oncol 2002;20:719–726. [PubMed: 11821453]

5. Heinrich S, Schäfer M, Weber A, Hany TF, Bhure U, Pestalozzi BC, et al. Neoadjuvant chemotherapy generates a significant tumor response in resectable pancreatic cancer without increasing morbidity: results of a prospective phase II trial. Ann Surg 2008;248:1014–1022. [PubMed: 19092346]
6. Rajan R, Poniecka A, Smith TL, Yang Y, Frye D, Pusztai L, et al. Change in tumor cellularity of breast carcinoma after neoadjuvant chemotherapy as a variable in the pathologic assessment of response. Cancer 2004;100:1365–1373. [PubMed: 15042669]
7. Vecchio FM, Valentini V, Minsky BD, Padula GD, Venkatraman ES, Balducci M, et al. The relationship of pathologic tumor regression grade (TRG) and outcomes after preoperative therapy in rectal cancer. Int J Radiat Oncol Biol Phys 2005;62:752–760. [PubMed: 15936556]
8. Goffin J, Baral S, Tu D, Nomikos D, Seymour L. Objective responses in patients with malignant melanoma or renal cell cancer in early clinical studies do not predict regulatory approval. Clin Cancer Res 2005;11:5928–5934. [PubMed: 16115935]
9. Ratain MJ, Eckhardt SG. Phase II studies of modern drugs directed against new targets: if you are fazed, too, then resist RECIST. J Clin Oncol 2004;22:4442–4445. [PubMed: 15483011]
10. Shepherd FA, Rodrigues Pereira J, Ciuleanu T, Tan EH, Hirsh V, Thongprasert S, et al. Erlotinib in previously treated non-small-cell lung cancer. N Engl J Med 2005;353:123–132. [PubMed: 16014882]
11. Ford R, Schwartz L, Dancey J, Dodd LE, Eisenhauer EA, Gwyther S, et al. Lessons learned from independent central review. Eur J Cancer 2009;45:268–274. [PubMed: 19101138]
12. Usami N, Iwano S, Yokoi K. Solitary fibrous tumor of the pleura: evaluation of the origin with 3D CT angiography. J Thorac Oncol 2007;2:1124–1125. [PubMed: 18090586]
13. McDonald DM, Choyke PL. Imaging of angiogenesis: from microscope to clinic. Nat Med 2003;9:713–725. [PubMed: 12778170]
14. van Vliet M, van Dijke CF, Wielopolski PA, ten Hagen TL, Veenland JF, Preda A, et al. MR angiography of tumor-related vasculature: from the clinic to the micro-environment. Radiographics 2005;25 Suppl 1:S85–S98. discussion S97–8. [PubMed: 16227499]
15. Boudghene FP, Gouny P, Tassart M, Callard P, Le Breton C, Vayssairat M. Subungual glomus tumor: combined use of MRI and three-dimensional contrast MR angiography. J Magn Reson Imaging 1998;8:1326–1328. [PubMed: 9848746]
16. Foote RL, Weidner N, Harris J, Hammond E, Lewis JE, Vuong T, et al. Evaluation of tumor angiogenesis measured with microvessel density (MVD) as a prognostic indicator in nasopharyngeal carcinoma: results of RTOG 9505. Int J Radiat Oncol Biol Phys 2005;61:745–753. [PubMed: 15708253]
17. El-Assal ON, Yamanoi A, Soda Y, Yamaguchi M, Igarashi M, Yamamoto A, et al. Clinical significance of microvessel density and vascular endothelial growth factor expression in hepatocellular carcinoma and surrounding liver: possible involvement of vascular endothelial growth factor in the angiogenesis of cirrhotic liver. Hepatology 1998;27:1554–1562. [PubMed: 9620326]
18. Giatromanolaki A, Koukourakis M, O'Byrne K, Fox S, White-house R, Talbot DC, et al. Prognostic value of angiogenesis in operable non-small cell lung cancer. J Pathol 1996;179:80–88. [PubMed: 8691350]
19. Miles KA. Tumour angiogenesis and its relation to contrast enhancement on computed tomography: a review. Eur J Radiol 1999;30:198–205. [PubMed: 10452718]
20. O'Connor JP, Jayson GC, Jackson A, Ghiorghiu D, Carrington BM, Rose CJ, et al. Enhancing fraction predicts clinical outcome following first-line chemotherapy in patients with epithelial ovarian carcinoma. Clin Cancer Res 2007;13:6130–6135. [PubMed: 17947478]
21. Braga L, Semelka RC, Pietrobon R, Martin D, de Barros N, Guller U. Does hypervascularity of liver metastases as detected on MRI predict disease progression in breast cancer patients? AJR Am J Roentgenol 2004;182:1207–1213. [PubMed: 15100120]
22. Chow KL, Gobin YP, Cloughesy T, Sayre JW, Villablanca JP, Viñuela F. Prognostic factors in recurrent glioblastoma multiforme and anaplastic astrocytoma treated with selective intraarterial chemotherapy. AJNR Am J Neuroradiol 2000;21:471–478. [PubMed: 10730637]

23. Hawighorst H, Knapstein PG, Knopp MV, Weikel W, Brix G, Zuna I, et al. Uterine cervical carcinoma: comparison of standard and pharmacokinetic analysis of time-intensity curves for assessment of tumor angiogenesis and patient survival. Cancer Res 1998;58:3598–3602. [PubMed: 9721867]
24. Mayr NA, Yuh WT, Magnotta VA, Ehrhardt JC, Wheeler JA, Sorosky JI, et al. Tumor perfusion studies using fast magnetic resonance imaging technique in advanced cervical cancer: a new noninvasive predictive assay. Int J Radiat Oncol Biol Phys 1996;36:623–633. [PubMed: 8948347]
25. Evelhoch JL. Key factors in the acquisition of contrast kinetic data for oncology. J Magn Reson Imaging 1999;10:254–259. [PubMed: 10508284]
26. Choyke PL, Dwyer AJ, Knopp MV. Functional tumor imaging with dynamic contrast-enhanced magnetic resonance imaging. J Magn Reson Imaging 2003;17:509–520. [PubMed: 12720260]
27. O'Connor JP, Jackson A, Parker GJ, Jayson GC. DCE-MRI biomarkers in the clinical evaluation of antiangiogenic and vascular disrupting agents. Br J Cancer 2007;96:189–195. [PubMed: 17211479]
28. Zee YK, O'Connor JP, Parker GJ, Jackson A, Clamp AR, Taylor MB, et al. Imaging angiogenesis of genitourinary tumors. Nat Rev Urol 2010;7:69–82. [PubMed: 20084077]
29. Miles KA, Charnsangavej C, Lee FT, Fishman EK, Horton K, Lee TY. Application of CT in the investigation of angiogenesis in oncology. Acad Radiol 2000;7:840–850. [PubMed: 11048881]
30. Hahn OM, Yang C, Medved M, Karczmar G, Kistner E, Karrison T, et al. Dynamic contrast-enhanced magnetic resonance imaging pharmacodynamic biomarker study of sorafenib in metastatic renal carcinoma. J Clin Oncol 2008;26:4572–4578. [PubMed: 18824708]
31. Marzola P, Degrassi A, Calderan L, Farace P, Crescimanno C, Nicolato E, et al. In vivo assessment of antiangiogenic activity of SU6668 in an experimental colon carcinoma model. Clin Cancer Res 2004;10:739–750. [PubMed: 14760097]
32. Kim S, Loevner LA, Quon H, Kilger A, Sherman E, Weinstein G, et al. Prediction of response to chemoradiation therapy in squamous cell carcinomas of the head and neck using dynamic contrast-enhanced MR imaging. AJNR Am J Neuroradiol 2010;31:262–268. [PubMed: 19797785]
33. Jensen LR, Huuse EM, Bathen TF, Goa PE, Bofin AM, Pedersen TB, et al. Assessment of early docetaxel response in an experimental model of human breast cancer using DCE-MRI, ex vivo HR MAS, and in vivo 1H MRS. NMR Biomed 2010;23:56–65. [PubMed: 19650073]
34. Morgan B, Thomas AL, Drevs J, Hennig J, Buchert M, Jivan A, et al. Dynamic contrast-enhanced magnetic resonance imaging as a biomarker for the pharmacological response of PTK787/ZK 222584, an inhibitor of the vascular endothelial growth factor receptor tyrosine kinases, in patients with advanced colorectal cancer and liver metastases: results from two phase I studies. J Clin Oncol 2003;21:3955–3964. [PubMed: 14517187]
35. Medved M, Karczmar G, Yang C, Dignam J, Gajewski TF, Kindler H, et al. Semiquantitative analysis of dynamic contrast enhanced MRI in cancer patients: variability and changes in tumor tissue over time. J Magn Reson Imaging 2004;20:122–128. [PubMed: 15221817]
36. Liu G, Rugo HS, Wilding G, McShane TM, Evelhoch JL, Ng C, et al. Dynamic contrast-enhanced magnetic resonance imaging as a pharmacodynamic measure of response after acute dosing of AG-013736, an oral angiogenesis inhibitor, in patients with advanced solid tumors: results from a phase I study. J Clin Oncol 2005;23:5464–5473. [PubMed: 16027440]
37. Paldino MJ, Barboriak DP. Fundamentals of quantitative dynamic contrast-enhanced MR imaging. Magn Reson Imaging Clin N Am 2009;17:277–289. [PubMed: 19406359]
38. Hanahan D, Weinberg RA. The hallmarks of cancer. Cell 2000;100:57–70. [PubMed: 10647931]
39. Chen X. Multimodality imaging of tumor integrin alphavbeta3 expression. Mini Rev Med Chem 2006;6:227–234. [PubMed: 16472190]
40. Cai W, Chen X. Multimodality imaging of vascular endothelial growth factor and vascular endothelial growth factor receptor expression. Front Biosci 2007;12:4267–4279. [PubMed: 17485373]
41. Cai W, Chen X. Multimodality molecular imaging of tumor angiogenesis. J Nucl Med 2008;49 Suppl 2:113S–128S. [PubMed: 18523069]
42. Cai W, Sam Gambhir S, Chen X. Multimodality tumor imaging targeting integrin alphavbeta3. Biotechniques 2005;39:S14–S25. [PubMed: 20158499]

43. Hillner BE, Siegel BA, Liu D, Shields AF, Gareen IF, Hanna L, et al. Impact of positron emission tomography/computed tomography and positron emission tomography (PET) alone on expected management of patients with cancer: initial results from the National Oncologic PET Registry. J Clin Oncol 2008;26:2155–2161. [PubMed: 18362365]
44. Wahl RL, Zasadny K, Helvie M, Hutchins GD, Weber B, Cody R. Metabolic monitoring of breast cancer chemohormonotherapy using positron emission tomography: initial evaluation. J Clin Oncol 1993;11:2101–2111. [PubMed: 8229124]
45. Larson SM, Schwartz LH. 18F-FDG PET as a candidate for “qualified biomarker”: functional assessment of treatment response in oncology. J Nucl Med 2006;47:901–903. [PubMed: 16741296]
46. Weber WA, Wieder H. Monitoring chemotherapy and radiotherapy of solid tumors. Eur J Nucl Med Mol Imaging 2006;33 Suppl 1:27–37. [PubMed: 16688451]
47. Weber WA. Assessing tumor response to therapy. J Nucl Med 2009;50 Suppl 1 1S-0.
48. de Geus-Oei LF, Vriens D, van Laarhoven HW, van der Graaf WT, Oyen WJ. Monitoring and predicting response to therapy with 18F-FDG PET in colorectal cancer: a systematic review. J Nucl Med 2009;50 Suppl 1:43S–54S. [PubMed: 19403879]
49. Brundage MD, Davies D, Mackillop WJ. Prognostic factors in non-small cell lung cancer: a decade of progress. Chest 2002;122:1037–1057. [PubMed: 12226051]
50. Hicks RJ. Role of 18F-FDG PET in assessment of response in non-small cell lung cancer. J Nucl Med 2009;50 Suppl 1:31S–42S. [PubMed: 19380411]
51. Mac Manus MP, Hicks RJ, Matthews JP, McKenzie A, Rischin D, Salminen EK, et al. Positron emission tomography is superior to computed tomography scanning for response-assessment after radical radiotherapy or chemoradiotherapy in patients with non-small-cell lung cancer. J Clin Oncol 2003;21:1285–1292. [PubMed: 12663716]
52. Avril N, Sassen S, Roylance R. Response to therapy in breast cancer. J Nucl Med 2009;50 Suppl 1:55S–63S. [PubMed: 19380410]
53. McDermott GM, Welch A, Staff RT, Gilbert FJ, Schweiger L, Semple SI, et al. Monitoring primary breast cancer throughout chemotherapy using FDG-PET. Breast Cancer Res Treat 2007;102:75–84. [PubMed: 16897427]
54. Krause BJ, Herrmann K, Wieder H, zum Büschenfelde CM. 18F-FDG PET and 18F-FDG PET/CT for assessing response to therapy in esophageal cancer. J Nucl Med 2009;50 Suppl 1:89S–96S. [PubMed: 19380406]
55. Klaeser B, Nitzsche E, Schuller JC, Köberle D, Widmer L, Balmer-Majno S, et al. Limited predictive value of FDG-PET for response assessment in the preoperative treatment of esophageal cancer: results of a prospective multi-center trial (SAKK 75/02). Onkologie 2009;32:724–730. [PubMed: 20016233]
56. Cheson BD, Pfistner B, Juweid ME, Gascoyne RD, Specht L, Horning SJ, et al. Revised response criteria for malignant lymphoma. J Clin Oncol 2007;25:579–586. [PubMed: 17242396]
57. Wahl RL, Jacene H, Kasamon Y, Lodge MA. From RECIST to PERCIST: evolving considerations for PET response criteria in solid tumors. J Nucl Med 2009;50 Suppl 1:122S–150S. [PubMed: 19403881]
58. Young H, Baum R, Cremerius U, Herholz K, Hoekstra O, Lammertsma AA, et al. Measurement of clinical and subclinical tumour response using [18F]-fluorodeoxyglucose and positron emission tomography: review and 1999 EORTC recommendations. European Organization for Research and Treatment of Cancer (EORTC) PET Study Group. Eur J Cancer 1999;35:1773–1782. [PubMed: 10673991]
59. Eisenhauer EA, Therasse P, Bogaerts J, Schwartz LH, Sargent D, Ford R, et al. New response evaluation criteria in solid tumours: revised RECIST guideline (version 1.1). Eur J Cancer 2009;45:228–247. [PubMed: 19097774]
60. Chen W, Silverman DH, Delaloye S, Czernin J, Kamdar N, Pope W, et al. 18F-FDOPA PET imaging of brain tumors: comparison study with 18F-FDG PET and evaluation of diagnostic accuracy. J Nucl Med 2006;47:904–911. [PubMed: 16741298]

61. Cheng YM, Ho CL, Chiu NT, Hsu KF. Cesarean section scar mimicking uterine malignant neoplasm at positron emission tomography/computed tomography. J Minim Invasive Gynecol 2009;16:372–374. [PubMed: 19423072]
62. Christman D, Crawford EJ, Friedkin M, Wolf AP. Detection of DNA synthesis in intact organisms with positron-emitting (methyl-11C)thymidine. Proc Natl Acad Sci U S A 1972;69:988–992. [PubMed: 4554538]
63. Rubini JR, Cronkite EP, Bond VP, Fliedner TM. The metabolism and fate of tritiated thymidine in man. J Clin Invest 1960;39:909–918. [PubMed: 14439902]
64. Bading JR, Shields AF. Imaging of cell proliferation: status and prospects. J Nucl Med 2008;49 Suppl 2:64S–80S. [PubMed: 18523066]
65. Shields AF, Grierson JR, Dohmen BM, Machulla HJ, Stayanoff JC, Lawhorn-Crews JM, et al. Imaging proliferation in vivo with [F-18]FLT and positron emission tomography. Nat Med 1998;4:1334–1336. [PubMed: 9809561]
66. Been LB, Suurmeijer AJ, Cobben DC, Jager PL, Hoekstra HJ, Elsinga PH. [18F]FLT-PET in oncology: current status and opportunities. Eur J Nucl Med Mol Imaging 2004;31:1659–1672. [PubMed: 15565331]
67. Yap CS, Czernin J, Fishbein MC, Cameron RB, Schiepers C, Phelps ME, et al. Evaluation of thoracic tumors with 18F-fluorothymidine and 18F-fluorodeoxyglucose-positron emission tomography. Chest 2006;129:393–401. [PubMed: 16478857]
68. Buck AK, Schirrmeister H, Hetzel M, Von Der Heide M, Halter G, Glatting G, et al. 3-deoxy-3-[(18)F]fluorothymidine-positron emission tomography for noninvasive assessment of proliferation in pulmonary nodules. Cancer Res 2002;62:3331–3334. [PubMed: 12067968]
69. Chen W, Cloughesy T, Kamdar N, Satyamurthy N, Bergsneider M, Liau L, et al. Imaging proliferation in brain tumors with 18F-FLT PET: comparison with 18F-FDG. J Nucl Med 2005;46:945–952. [PubMed: 15937304]
70. Kenny LM, Vigushin DM, Al-Nahhas A, Osman S, Luthra SK, Shousha S, et al. Quantification of cellular proliferation in tumor and normal tissues of patients with breast cancer by [18F] fluorothymidine-positron emission tomography imaging: evaluation of analytical methods. Cancer Res 2005;65:10104–10112. [PubMed: 16267037]
71. van Westreenen HL, Cobben DC, Jager PL, van Dullemen HM, Wesseling J, Elsinga PH, et al. Comparison of 18F-FLT PET and 18F-FDG PET in esophageal cancer. J Nucl Med 2005;46:400–404. [PubMed: 15750150]
72. de Langen AJ, Klabbers B, Lubberink M, Boellaard R, Spreeuwenberg MD, Slotman BJ, et al. Reproducibility of quantitative 18F-3′-deoxy-3′-fluorothymidine measurements using positron emission tomography. Eur J Nucl Med Mol Imaging 2009;36:389–395. [PubMed: 18931838]
73. Yang YJ, Ryu JS, Kim SY, Oh SJ, Im KC, Lee H, et al. Use of 3′-deoxy-3′-[18F]fluorothymidine PET to monitor early responses to radiation therapy in murine SCCVII tumors. Eur J Nucl Med Mol Imaging 2006;33:412–419. [PubMed: 16404598]
74. Sugiyama M, Sakahara H, Sato K, Harada N, Fukumoto D, Kakiuchi T, et al. Evaluation of 3′-deoxy-3′-18F-fluorothymidine for monitoring tumor response to radiotherapy and photodynamic therapy in mice. J Nucl Med 2004;45:1754–1758. [PubMed: 15471845]
75. Molthoff CF, Klabbers BM, Berkhof J, Felten JT, van Gelder M, Windhorst AD, et al. Monitoring response to radiotherapy in human squamous cell cancer bearing nude mice: comparison of 2′-deoxy-2′-[18F]fluoro-D-glucose (FDG) and 3′-[18F]fluoro-3′-deoxythymidine (FLT). Mol Imaging Biol 2007;9:340–347. [PubMed: 17643202]
76. Buck AK, Kratochwil C, Glatting G, Juweid M, Bommer M, Tepsic D, et al. Early assessment of therapy response in malignant lymphoma with the thymidine analogue [18F]FLT. Eur J Nucl Med Mol Imaging 2007;34:1775–1782. [PubMed: 17541585]
77. Pan MH, Huang SC, Liao YP, Schaue D, Wang CC, Stout DB, et al. FLT-PET imaging of radiation responses in murine tumors. Mol Imaging Biol 2008;10:325–334. [PubMed: 18670825]
78. Buck AK, Halter G, Schirrmeister H, Kotzerke J, Wurziger I, Glatting G, et al. Imaging proliferation in lung tumors with PET: 18F-FLT versus 18F-FDG. J Nucl Med 2003;44:1426–1431. [PubMed: 12960187]

79. Choi SJ, Kim JS, Kim JH, Oh SJ, Lee JG, Kim CJ, et al. [18F]3′-deoxy-3′-fluorothymidine PET for the diagnosis and grading of brain tumors. Eur J Nucl Med Mol Imaging 2005;32:653–659. [PubMed: 15711980]
80. Kenny L, Coombes RC, Vigushin DM, Al-Nahhas A, Shousha S, Aboagye EO. Imaging early changes in proliferation at 1 week post chemotherapy: a pilot study in breast cancer patients with 3′-deoxy-3′-[18F]fluorothymidine positron emission tomography. Eur J Nucl Med Mol Imaging 2007;34:1339–1347. [PubMed: 17333178]
81. Sohn HJ, Yang YJ, Ryu JS, Oh SJ, Im KC, Moon DH, et al. [18F]Fluorothymidine positron emission tomography before and 7 days after gefitinib treatment predicts response in patients with advanced adenocarcinoma of the lung. Clin Cancer Res 2008;14:7423–7429. [PubMed: 19010859]
82. Muzi M, Vesselle H, Grierson JR, Mankoff DA, Schmidt RA, Peterson L, et al. Kinetic analysis of 3′-deoxy-3′-fluorothymidine PET studies: validation studies in patients with lung cancer. J Nucl Med 2005;46:274–282. [PubMed: 15695787]
83. Troost EG, Vogel WV, Merkx MA, Slootweg PJ, Marres HA, Peeters WJ, et al. 18F-FLT PET does not discriminate between reactive and metastatic lymph nodes in primary head and neck cancer patients. J Nucl Med 2007;48:726–735. [PubMed: 17475960]
84. Schwartz JL, Tamura Y, Jordan R, Grierson JR, Krohn KA. Monitoring tumor cell proliferation by targeting DNA synthetic processes with thymidine and thymidine analogs. J Nucl Med 2003;44:2027–2032. [PubMed: 14660729]
85. Reske SN, Deisenhofer S. Is 3′-deoxy-3′-(18)F-fluorothymidine a better marker for tumour response than (18)F-fluorodeoxyglucose? Eur J Nucl Med Mol Imaging 2006;33 Suppl 1:38–43. [PubMed: 16721567]
86. Leenders WP, Küsters B, de Waal RM. Vessel co-option: how tumors obtain blood supply in the absence of sprouting angiogenesis. Endothelium 2002;9:83–87. [PubMed: 12200959]
87. Folkman J. Tumor angiogenesis: therapeutic implications. N Engl J Med 1971;285:1182–1186. [PubMed: 4938153]
88. Yancopoulos GD, Davis S, Gale NW, Rudge JS, Wiegand SJ, Holash J. Vascular-specific growth factors and blood vessel formation. Nature 2000;407:242–248. [PubMed: 11001067]
89. Auguste P, Lemiere S, Larrieu-Lahargue F, Bikfalvi A. Molecular mechanisms of tumor vascularization. Crit Rev Oncol Hematol 2005;54:53–61. [PubMed: 15780907]
90. Herbst RS, Mullani NA, Davis DW, Hess KR, McConkey DJ, Charnsangavej C, et al. Development of biologic markers of response and assessment of antiangiogenic activity in a clinical trial of human recombinant endostatin. J Clin Oncol 2002;20:3804–3814. [PubMed: 12228200]
91. Hood JD, Cheresh DA. Role of integrins in cell invasion and migration. Nat Rev Cancer 2002;2:91–100. [PubMed: 12635172]
92. Brooks PC, Clark RA, Cheresh DA. Requirement of vascular integrin alpha v beta 3 for angiogenesis. Science 1994;264:569–571. [PubMed: 7512751]
93. Hynes RO. Integrins: bidirectional, allosteric signaling machines. Cell 2002;110:673–687. [PubMed: 12297042]
94. Ruoslahti E, Pierschbacher MD. New perspectives in cell adhesion: RGD and integrins. Science 1987;238:491–497. [PubMed: 2821619]
95. Pepper MS. Role of the matrix metalloproteinase and plasminogen activator-plasmin systems in angiogenesis. Arterioscler Thromb Vasc Biol 2001;21:1104–1117. [PubMed: 11451738]
96. Hynes RO, Bader BL, Hodivala-Dilke K. Integrins in vascular development. Braz J Med Biol Res 1999;32:501–510. [PubMed: 10412560]
97. Cai W, Chen X. Anti-angiogenic cancer therapy based on integrin alphavbeta3 antagonism. Anticancer Agents Med Chem 2006;6:407–428. [PubMed: 17017851]
98. Mizejewski GJ. Role of integrins in cancer: survey of expression patterns. Proc Soc Exp Biol Med 1999;222:124–138. [PubMed: 10564536]
99. Haubner R, Wester HJ, Reuning U, Senekowitsch-Schmidtke R, Diefenbach B, Kessler H, et al. Radiolabeled alpha(v)beta3 integrin antagonists: a new class of tracers for tumor targeting. J Nucl Med 1999;40:1061–1071. [PubMed: 10452325]

100. Chen X, Park R, Shahinian AH, Bading JR, Conti PS. Pharmacokinetics and tumor retention of 125I-labeled RGD peptide are improved by PEGylation. Nucl Med Biol 2004;31:11–19. [PubMed: 14741566]
101. Haubner R. Alphavbeta3-integrin imaging: a new approach to characterise angiogenesis? Eur J Nucl Med Mol Imaging 2006;33 Suppl 1:54–63. [PubMed: 16791598]
102. Gurrath M, Müller G, Kessler H, Aumailley M, Timpl R. Conformation/activity studies of rationally designed potent antiadhesive RGD peptides. Eur J Biochem 1992;210:911–921. [PubMed: 1483474]
103. van Hagen PM, Breeman WA, Bernard HF, Schaar M, Mooij CM, Srinivasan A, et al. Evaluation of a radiolabelled cyclic DTPA-RGD analogue for tumour imaging and radionuclide therapy. Int J Cancer 2000;90:186–198. [PubMed: 10993959]
104. Chen X, Hou Y, Tohme M, Park R, Khankaldyyan V, Gonzales-Gomez I, et al. Pegylated Arg-Gly-Asp peptide: 64Cu labeling and PET imaging of brain tumor alphavbeta3-integrin expression. J Nucl Med 2004;45:1776–1783. [PubMed: 15471848]
105. Li ZB, Chen K, Chen X. (68)Ga-labeled multimeric RGD peptides for microPET imaging of integrin alpha(v)beta (3) expression. Eur J Nucl Med Mol Imaging 2008;35:1100–1108. [PubMed: 18204838]
106. Noiri E, Goligorsky MS, Wang GJ, Wang J, Cabahug CJ, Sharma S, et al. Biodistribution and clearance of 99mTc-labeled Arg-Gly-Asp (RGD) peptide in rats with ischemic acute renal failure. J Am Soc Nephrol 1996;7:2682–2688. [PubMed: 8989749]
107. Beer AJ, Haubner R, Goebel M, Luderschmidt S, Spilker ME, Wester HJ, et al. Biodistribution and pharmacokinetics of the alphavbeta3-selective tracer 18F-galacto-RGD in cancer patients. J Nucl Med 2005;46:1333–1341. [PubMed: 16085591]
108. Beer AJ, Haubner R, Wolf I, Goebel M, Luderschmidt S, Niemeyer M, et al. PET-based human dosimetry of 18F-galacto-RGD, a new radiotracer for imaging alpha v beta3 expression. J Nucl Med 2006;47:763–769. [PubMed: 16644745]
109. Beer AJ, Haubner R, Sarbia M, Goebel M, Luderschmidt S, Grosu AL, et al. Positron emission tomography using [18F] Galacto-RGD identifies the level of integrin alpha(v)beta3 expression in man. Clin Cancer Res 2006;12:3942–3949. [PubMed: 16818691]
110. Beer AJ, Lorenzen S, Metz S, Herrmann K, Watzlowik P, Wester HJ, et al. Comparison of integrin alphaVbeta3 expression and glucose metabolism in primary and metastatic lesions in cancer patients: a PET study using 18F-galacto-RGD and 18F-FDG. J Nucl Med 2008;49:22–29. [PubMed: 18077538]
111. Liu S, Hsieh WY, Jiang Y, Kim YS, Sreerama SG, Chen X, et al. Evaluation of a (99m)Tc-labeled cyclic RGD tetramer for noninvasive imaging integrin alpha(v)beta3-positive breast cancer. Bioconjug Chem 2007;18:438–446. [PubMed: 17341108]
112. Li ZB, Cai W, Cao Q, Chen K, Wu Z, He L, et al. (64)Cu-labeled tetrameric and octameric RGD peptides for small-animal PET of tumor alpha(v)beta(3) integrin expression. J Nucl Med 2007;48:1162–1171. [PubMed: 17574975]
113. Liu Z, Liu S, Wang F, Chen X. Noninvasive imaging of tumor integrin expression using (18)F-labeled RGD dimer peptide with PEG(4) linkers. Eur J Nucl Med Mol Imaging 2009;36:1296–1307. [PubMed: 19296102]
114. Kim S, Bell K, Mousa SA, Varner JA. Regulation of angiogenesis in vivo by ligation of integrin alpha5beta1 with the central cell-binding domain of fibronectin. Am J Pathol 2000;156:1345–1362. [PubMed: 10751360]
115. Renner W, Pilger E. Simultaneous in vivo quantitation of vascular endothelial growth factor mRNA splice variants. J Vasc Res 1999;36:133–1338. [PubMed: 10213909]
116. Houck KA, Leung DW, Rowland AM, Winer J, Ferrara N. Dual regulation of vascular endothelial growth factor bioavailability by genetic and proteolytic mechanisms. J Biol Chem 1992;267:26031–26037. [PubMed: 1464614]
117. Ferrara N. The role of VEGF in the regulation of physiological and pathological angiogenesis. EXS 2005;94:209–231. [PubMed: 15617481]
118. Shibuya M, Claesson-Welsh L. Signal transduction by VEGF receptors in regulation of angiogenesis and lymphangiogenesis. Exp Cell Res 2006;312:549–560. [PubMed: 16336962]

119. Ferrara N. Vascular endothelial growth factor: basic science and clinical progress. Endocr Rev 2004;25:581–611. [PubMed: 15294883]
120. Nagengast WB, de Vries EG, Hospers GA, Mulder NH, de Jong JR, Hollema H, et al. In vivo VEGF imaging with radiolabeled bevacizumab in a human ovarian tumor xenograft. J Nucl Med 2007;48:1313–1319. [PubMed: 17631557]
121. Jayson GC, Zweit J, Jackson A, Mulatero C, Julyan P, Ranson M, et al. Molecular imaging and biological evaluation of HuMV833 anti-VEGF antibody: implications for trial design of antiangiogenic antibodies. J Natl Cancer Inst 2002;94:1484–1493. [PubMed: 12359857]
122. Scheer MG, Stollman TH, Boerman OC, Verrijp K, Sweep FC, Leenders WP, et al. Imaging liver metastases of colorectal cancer patients with radiolabelled bevacizumab: lack of correlation with VEGF-A expression. Eur J Cancer 2008;44:1835–1840. [PubMed: 18632262]
123. Cai W, Chen K, Mohamedali KA, Cao Q, Gambhir SS, Rosenblum MG, et al. PET of vascular endothelial growth factor receptor expression. J Nucl Med 2006;47:2048–2056. [PubMed: 17138749]
124. Chen K, Cai W, Li ZB, Wang H, Chen X. Quantitative PET imaging of VEGF receptor expression. Mol Imaging Biol 2009;11:15–22. [PubMed: 18784964]
125. Hsu AR, Cai W, Veeravagu A, Mohamedali KA, Chen K, Kim S, et al. Multimodality molecular imaging of glioblastoma growth inhibition with vasculature-targeting fusion toxin VEGF121/rGel. J Nucl Med 2007;48:445–454. [PubMed: 17332623]
126. George SJ. Therapeutic potential of matrix metalloproteinase inhibitors in atherosclerosis. Expert Opin Investig Drugs 2000;9:993–1007.
127. Folgueras AR, Pendás AM, Sánchez LM, López-Otin C. Matrix metalloproteinases in cancer: from new functions to improved inhibition strategies. Int J Dev Biol 2004;48:411–424. [PubMed: 15349816]
128. Galis ZS, Khatri JJ. Matrix metalloproteinases in vascular remodeling and atherogenesis: the good, the bad, and the ugly. Circ Res 2002;90:251–262. [PubMed: 11861412]
129. Pellikainen JM, Ropponen KM, Kataja VV, Kellokoski JK, Eskelinen MJ, Kosma VM. Expression of matrix metalloproteinase (MMP)-2 and MMP-9 in breast cancer with a special reference to activator protein-2, HER2, and prognosis. Clin Cancer Res 2004;10:7621–7628. [PubMed: 15569994]
130. Juuti A, Lundin J, Nordling S, Louhimo J, Haglund C. Epithelial MMP-2 expression correlates with worse prognosis in pancreatic cancer. Oncology 2006;71:61–68. [PubMed: 17377415]
131. Lee LY, Wu CM, Wang CC, Yu JS, Liang Y, Huang KH, et al. Expression of matrix metalloproteinases MMP-2 and MMP-9 in gastric cancer and their relation to claudin-4 expression. Histol Histopathol 2008;23:515–521. [PubMed: 18283635]
132. Koivunen E, Arap W, Valtanen H, Rainisalo A, Medina OP, Heikkilä P, et al. Tumor targeting with a selective gelatinase inhibitor. Nat Biotechnol 1999;17:768–774. [PubMed: 10429241]
133. Hanaoka H, Mukai T, Habashita S, Asano D, Ogawa K, Kuroda Y, et al. Chemical design of a radiolabeled gelatinase inhibitor peptide for the imaging of gelatinase activity in tumors. Nucl Med Biol 2007;34:503–510. [PubMed: 17591550]
134. Sprague JE, Li WP, Liang K, Achilefu S, Anderson CJ. In vitro and in vivo investigation of matrix metalloproteinase expression in metastatic tumor models. Nucl Med Biol 2006;33:227–237. [PubMed: 16546677]
135. MacPherson LJ, Bayburt EK, Capparelli MP, Carroll BJ, Goldstein R, Justice MR, et al. Discovery of CGS 27023A, a non-peptidic, potent, and orally active stromelysin inhibitor that blocks cartilage degradation in rabbits. J Med Chem 1997;40:2525–2532. [PubMed: 9258358]
136. Scozzafava A, Supuran CT. Carbonic anhydrase and matrix metalloproteinase inhibitors: sulfonylated amino acid hydroxamates with MMP inhibitory properties act as efficient inhibitors of CA isozymes I, II, and IV, and N-hydroxysulfonamides inhibit both these zinc enzymes. J Med Chem 2000;43:3677–3687. [PubMed: 11020282]
137. Zheng QH, Fei X, Liu X, Wang JQ, Bin Sun H, Mock BH, et al. Synthesis and preliminary biological evaluation of MMP inhibitor radiotracers [11C]methyl-halo-CGS 27023A analogs, new potential PET breast cancer imaging agents. Nucl Med Biol 2002;29:761–770. [PubMed: 12381456]

138. Zheng QH, Fei X, DeGrado TR, Wang JQ, Stone KL, Martinez TD, et al. Synthesis, biodistribution and micro-PET imaging of a potential cancer biomarker carbon-11 labeled MMP inhibitor (2R)-2-[[4-(6-fluorohex-1-ynyl)phenyl]sulfonylamino]-3-methyl-butyric acid [11C]methyl ester. Nucl Med Biol 2003;30:753–760. [PubMed: 14499334]
139. Neri D, Carnemolla B, Nissim A, Leprini A, Querzè G, Balza E, et al. Targeting by affinity-matured recombinant antibody fragments of an angiogenesis associated fibronectin isoform. Nat Biotechnol 1997;15:1271–1275. [PubMed: 9359110]
140. Pini A, Viti F, Santucci A, Carnemolla B, Zardi L, Neri P, et al. Design and use of a phage display library. Human antibodies with subnanomolar affinity against a marker of angiogenesis eluted from a two-dimensional gel. J Biol Chem 1998;273:21769–21776. [PubMed: 9705314]
141. Santimaria M, Moscatelli G, Viale GL, Giovannoni L, Neri G, Viti F, et al. Immunoscintigraphic detection of the ED-B domain of fibronectin, a marker of angiogenesis, in patients with cancer. Clin Cancer Res 2003;9:571–579. [PubMed: 12576420]
142. Carnemolla B, Castellani P, Ponassi M, Borsi L, Urbini S, Nicolo G, et al. Identification of a glioblastoma-associated tenascin-C isoform by a high affinity recombinant antibody. Am J Pathol 1999;154:1345–1352. [PubMed: 10329587]
143. Silacci M, Brack SS, Späth N, Buck A, Hillinger S, Arni S, et al. Human monoclonal antibodies to domain C of tenascin-C selectively target solid tumors in vivo. Protein Eng Des Sel 2006;19:471–478. [PubMed: 16928692]
144. Marron MB, Singh H, Tahir TA, Kavumkal J, Kim HZ, Koh GY, et al. Regulated proteolytic processing of Tie1 modulates ligand responsiveness of the receptor-tyrosine kinase Tie2. J Biol Chem 2007;282:30509–30517. [PubMed: 17728252]
145. Seaman S, Stevens J, Yang MY, Logsdon D, Graff-Cherry C, St Croix B. Genes that distinguish physiological and pathological angiogenesis. Cancer Cell 2007;11:539–554. [PubMed: 17560335]
146. Brizel DM, Scully SP, Harrelson JM, Layfield LJ, Bean JM, Prosnitz LR, et al. Tumor oxygenation predicts for the likelihood of distant metastases in human soft tissue sarcoma. Cancer Res 1996;56:941–943. [PubMed: 8640781]
147. Höckel M, Knoop C, Schlenger K, Vorndran B, Baussmann E, Mitze M, et al. Intratumoral pO2 predicts survival in advanced cancer of the uterine cervix. Radiother Oncol 1993;26:45–50. [PubMed: 8438086]
148. Souvatzoglou M, Grosu AL, Röper B, Krause BJ, Beck R, Reischl G, et al. Tumour hypoxia imaging with [18F]FAZA PET in head and neck cancer patients: a pilot study. Eur J Nucl Med Mol Imaging 2007;34:1566–1575. [PubMed: 17447061]
149. Vaupel P, Mayer A. Hypoxia in cancer: significance and impact on clinical outcome. Cancer Metastasis Rev 2007;26:225–239. [PubMed: 17440684]
150. Ljungkvist AS, Bussink J, Kaanders JH, van der Kogel AJ. Dynamics of tumor hypoxia measured with bioreductive hypoxic cell markers. Radiat Res 2007;167:127–145. [PubMed: 17390721]
151. Lucignani G. PET imaging with hypoxia tracers: a must in radiation therapy. Eur J Nucl Med Mol Imaging 2008;35:838–842. [PubMed: 18264705]
152. Gallez B, Baudelet C, Jordan BF. Assessment of tumor oxygenation by electron paramagnetic resonance: principles and applications. NMR Biomed 2004;17:240–262. [PubMed: 15366026]
153. Dunn JF, O'Hara JA, Zaim-Wadghiri Y, Lei H, Meyerand ME, Grinberg OY, et al. Changes in oxygenation of intracranial tumors with carbogen: a BOLD MRI and EPR oximetry study. J Magn Reson Imaging 2002;16:511–521. [PubMed: 12412027]
154. Padhani A. PET imaging of tumour hypoxia. Cancer Imaging 2006;6:S117–S121. [PubMed: 17114063]
155. Nehmeh SA, Lee NY, Schröder H, Squire O, Zanzonico PB, Erdi YE, et al. Reproducibility of intratumor distribution of (18)F-fluoromisonidazole in head and neck cancer. Int J Radiat Oncol Biol Phys 2008;70:235–242. [PubMed: 18086391]
156. Rajendran JG, Schwartz DL, O'Sullivan J, Peterson LM, Ng P, Scharnhorst J, et al. Tumor hypoxia imaging with [F-18] fluoromisonidazole positron emission tomography in head and neck cancer. Clin Cancer Res 2006;12:5435–5441. [PubMed: 17000677]

157. Rischin D, Hicks RJ, Fisher R, Binns D, Corry J, Porceddu S, et al. Prognostic significance of [18F]-misonidazole positron emission tomography-detected tumor hypoxia in patients with advanced head and neck cancer randomly assigned to chemoradiation with or without tirapazamine: a substudy of Trans-Tasman Radiation Oncology Group Study 98.02. J Clin Oncol 2006;24:2098–2104. [PubMed: 16648512]
158. Spence AM, Muzi M, Swanson KR, O'Sullivan F, Rockhill JK, Rajendran JG, et al. Regional hypoxia in glioblastoma multiforme quantified with [18F]fluoromisonidazole positron emission tomography before radiotherapy: correlation with time to progression and survival. Clin Cancer Res 2008;14:2623–2630. [PubMed: 18451225]
159. Eschmann SM, Paulsen F, Reimold M, Dittmann H, Welz S, Reischl G, et al. Prognostic impact of hypoxia imaging with 18F-misonidazole PET in non-small cell lung cancer and head and neck cancer before radiotherapy. J Nucl Med 2005;46:253–260. [PubMed: 15695784]
160. Rajendran JG, Hendrickson KR, Spence AM, Muzi M, Krohn KA, Mankoff DA. Hypoxia imaging-directed radiation treatment planning. Eur J Nucl Med Mol Imaging 2006;33 Suppl 1:44–53. [PubMed: 16763816]
161. Reischl G, Dorow DS, Cullinane C, Katsifis A, Roselt P, Binns D, et al. Imaging of tumor hypoxia with [124I]IAZA in comparison with [18F]FMISO and [18F]FAZA—first small animal PET results. J Pharm Pharm Sci 2007;10:203–211. [PubMed: 17706178]
162. Evans SM, Fraker D, Hahn SM, Gleason K, Jenkins WT, Jenkins K, et al. EF5 binding and clinical outcome in human soft tissue sarcomas. Int J Radiat Oncol Biol Phys 2006;64:922–927. [PubMed: 16458778]
163. Evans SM, Judy KD, Dunphy I, Jenkins WT, Nelson PT, Collins R, et al. Comparative measurements of hypoxia in human brain tumors using needle electrodes and EF5 binding. Cancer Res 2004;64:1886–1892. [PubMed: 14996753]
164. Minn H, Grönroos TJ, Komar G, Eskola O, Lehtiö K, Tuomela J, et al. Imaging of tumor hypoxia to predict treatment sensitivity. Curr Pharm Des 2008;14:2932–2942. [PubMed: 18991711]
165. Kaneta T, Takai Y, Iwata R, Hakamatsuka T, Yasuda H, Nakayama K, et al. Initial evaluation of dynamic human imaging using 18F-FRP170 as a new PET tracer for imaging hypoxia. Ann Nucl Med 2007;21:101–107. [PubMed: 17424976]
166. Lewis JS, McCarthy DW, McCarthy TJ, Fujibayashi Y, Welch MJ. Evaluation of 64Cu-ATSM in vitro and in vivo in a hypoxic tumor model. J Nucl Med 1999;40:177–183. [PubMed: 9935074]
167. Fujibayashi Y, Taniuchi H, Yonekura Y, Ohtani H, Konishi J, Yokoyama A. Copper-62-ATSM: a new hypoxia imaging agent with high membrane permeability and low redox potential. J Nucl Med 1997;38:1155–1160. [PubMed: 9225812]
168. Lewis JS, Herrero P, Sharp TL, Engelbach JA, Fujibayashi Y, Laforest R, et al. Delineation of hypoxia in canine myocardium using PET and copper(II)-diacetyl-bis(N(4)-methylthiosemicarbazone). J Nucl Med 2002;43:1557–1569. [PubMed: 12411560]
169. Takahashi N, Fujibayashi Y, Yonekura Y, Welch MJ, Waki A, Tsuchida T, et al. Copper-62 ATSM as a hypoxic tissue tracer in myocardial ischemia. Ann Nucl Med 2001;15:293–296. [PubMed: 11545205]
170. Takahashi N, Fujibayashi Y, Yonekura Y, Welch MJ, Waki A, Tsuchida T, et al. Evaluation of 62Cu labeled diacetyl-bis(N4-methylthiosemicarbazone) as a hypoxic tissue tracer in patients with lung cancer. Ann Nucl Med 2000;14:323–328. [PubMed: 11108159]
171. Dietz DW, Dehdashti F, Grigsby PW, Malyapa RS, Myerson RJ, Picus J, et al. Tumor hypoxia detected by positron emission tomography with 60Cu-ATSM as a predictor of response and survival in patients undergoing neoadjuvant chemoradiotherapy for rectal carcinoma: a pilot study. Dis Colon Rectum 2008;51:1641–1648. [PubMed: 18682881]
172. Dehdashti F, Grigsby PW, Mintun MA, Lewis JS, Siegel BA, Welch MJ. Assessing tumor hypoxia in cervical cancer by positron emission tomography with 60Cu-ATSM: relationship to therapeutic response-a preliminary report. Int J Radiat Oncol Biol Phys 2003;55:1233–1238. [PubMed: 12654432]
173. Lewis JS, Laforest R, Dehdashti F, Grigsby PW, Welch MJ, Siegel BA. An imaging comparison of 64Cu-ATSM and 60Cu-ATSM in cancer of the uterine cervix. J Nucl Med 2008;49:1177–1182. [PubMed: 18552145]

174. Lohith TG, Kudo T, Demura Y, Umeda Y, Kiyono Y, Fujibayashi Y, et al. Pathophysiologic correlation between 62Cu-ATSM and 18F-FDG in lung cancer. J Nucl Med 2009;50:1948–1953. [PubMed: 19910425]

175. Yuan H, Schroeder T, Bowsher JE, Hedlund LW, Wong T, Dewhirst MW. Intertumoral differences in hypoxia selectivity of the PET imaging agent 64Cu(II)-diacetyl-bis(N4-methylthiosemicarbazone). J Nucl Med 2006;47:989–998. [PubMed: 16741309]

176. Kerr JF, Wyllie AH, Currie AR. Apoptosis: a basic biological phenomenon with wide-ranging implications in tissue kinetics. Br J Cancer 1972;26:239–257. [PubMed: 4561027]

177. Fadok VA, Voelker DR, Campbell PA, Cohen JJ, Bratton DL, Henson PM. Exposure of phosphatidylserine on the surface of apoptotic lymphocytes triggers specific recognition and removal by macrophages. J Immunol 1992;148:2207–2216. [PubMed: 1545126]

178. Thompson CB. Apoptosis in the pathogenesis and treatment of disease. Science 1995;267:1456–1462. [PubMed: 7878464]

179. Hersey P, Zhang XD, Mhaidat N. Overcoming resistance to apoptosis in cancer therapy. Adv Exp Med Biol 2008;615:105–126. [PubMed: 18437893]

180. Emoto K, Toyama-Sorimachi N, Karasuyama H, Inoue K, Umeda M. Exposure of phosphatidylethanolamine on the surface of apoptotic cells. Exp Cell Res 1997;232:430–434. [PubMed: 9168822]

181. Zwaal RF, Comfurius P, Bevers EM. Surface exposure of phosphatidylserine in pathological cells. Cell Mol Life Sci 2005;62:971–988. [PubMed: 15761668]

182. Martin SJ, Reutelingsperger CP, McGahon AJ, Rader JA, van Schie RC, LaFace DM, et al. Early redistribution of plasma membrane phosphatidylserine is a general feature of apoptosis regardless of the initiating stimulus: inhibition by overexpression of Bcl-2 and Abl. J Exp Med 1995;182:1545–1556. [PubMed: 7595224]

183. van Engeland M, Kuijpers HJ, Ramaekers FC, Reutelingsperger CP, Schutte B. Plasma membrane alterations and cytoskeletal changes in apoptosis. Exp Cell Res 1997;235:421–430. [PubMed: 9299167]

184. Blankenberg FG, Katsikis PD, Tait JF, Davis RE, Naumovski L, Ohtsuki K, et al. Imaging of apoptosis (programmed cell death) with 99mTc annexin V. J Nucl Med 1999;40:184–191. [PubMed: 9935075]

185. Blankenberg FG, Katsikis PD, Tait JF, Davis RE, Naumovski L, Ohtsuki K, et al. In vivo detection and imaging of phosphatidylserine expression during programmed cell death. Proc Natl Acad Sci U S A 1998;95:6349–6354. [PubMed: 9600968]

186. Belhocine T, Steinmetz N, Hustinx R, Bartsch P, Jerusalem G, Seidel L, et al. Increased uptake of the apoptosis-imaging agent (99m)Tc recombinant human Annexin V in human tumors after one course of chemotherapy as a predictor of tumor response and patient prognosis. Clin Cancer Res 2002;8:2766–2774. [PubMed: 12231515]

187. Boersma HH, Liem IH, Kemerink GJ, Thimister PW, Hofstra L, Stolk LM, et al. Comparison between human pharmacokinetics and imaging properties of two conjugation methods for 99mTc-annexin A5. Br J Radiol 2003;76:553–560. [PubMed: 12893698]

188. Kemerink GJ, Liu X, Kieffer D, Ceyssens S, Mortelmans L, Verbruggen AM, et al. Safety, biodistribution, and dosimetry of 99mTc-HYNIC-annexin V, a novel human recombinant annexin V for human application. J Nucl Med 2003;44:947–952. [PubMed: 12791824]

189. Van den Brande JM, Koehler TC, Zelinkova Z, Bennink RJ, te Velde AA, ten Cate FJ, et al. Prediction of antitumour necrosis factor clinical efficacy by real-time visualisation of apoptosis in patients with Crohn's disease. Gut 2007;56:509–517. [PubMed: 17082252]

190. Belhocine T, Steinmetz N, Li C, Green A, Blankenberg FG. The imaging of apoptosis with the radiolabeled annexin V: optimal timing for clinical feasibility. Technol Cancer Res Treat 2004;3:23–32. [PubMed: 14750890]

191. Kartachova M, van Zandwijk N, Burgers S, van Tinteren H, Verheij M, Valdés Olmos RA. Prognostic significance of 99mTc Hynic-rh-annexin V scintigraphy during platinum-based chemotherapy in advanced lung cancer. J Clin Oncol 2007;25:2534–2539. [PubMed: 17577031]

192. Kartachova MS, Valdés Olmos RA, Haas RL, Hoebers FJ, van Herk M, Verheij M. 99mTc-HYNIC-rh-annexin-V scintigraphy: visual and quantitative evaluation of early treatment-induced

apoptosis to predict treatment outcome. Nucl Med Commun 2008;29:39–44. [PubMed: 18049096]

193. van de Wiele C, Lahorte C, Vermeersch H, Loose D, Mervillie K, Steinmetz ND, et al. Quantitative tumor apoptosis imaging using technetium-99m-HYNIC annexin V single photon emission computed tomography. J Clin Oncol 2003;21:3483–3487. [PubMed: 12972524]
194. Haas RL, de Jong D, Valdés Olmos RA, Hoefnagel CA, van den Heuvel I, Zerp SF, et al. In vivo imaging of radiation-induced apoptosis in follicular lymphoma patients. Int J Radiat Oncol Biol Phys 2004;59:782–787. [PubMed: 15183481]
195. Rottey S, Slegers G, Van Belle S, Goethals I, Van de Wiele C. Sequential 99mTc-hydrazinonicotinamide-annexin V imaging for predicting response to chemotherapy. J Nucl Med 2006;47:1813–1818. [PubMed: 17079815]
196. Tait JF, Smith C, Blankenberg FG. Structural requirements for in vivo detection of cell death with 99mTc-annexin V. J Nucl Med 2005;46:807–815. [PubMed: 15872355]
197. Tait JF, Smith C, Levashova Z, Patel B, Blankenberg FG, Vanderheyden JL. Improved detection of cell death in vivo with annexin V radiolabeled by site-specific methods. J Nucl Med 2006;47:1546–1553. [PubMed: 16954565]
198. Wang F, Fang W, Zhao M, Wang Z, Ji S, Li Y, et al. Imaging paclitaxel (chemotherapy)-induced tumor apoptosis with 99mTc C2A, a domain of synaptotagmin I: a preliminary study. Nucl Med Biol 2008;35:359–364. [PubMed: 18355692]
199. Iwamoto K, Hayakawa T, Murate M, Makino A, Ito K, Fujisawa T, et al. Curvature-dependent recognition of ethanolamine phospholipids by duramycin and cinnamycin. Biophys J 2007;93:1608–1619. [PubMed: 17483159]
200. Zhou D, Chu W, Rothfuss J, Zeng C, Xu J, Jones L, et al. Synthesis, radiolabeling, and in vivo evaluation of an 18F-labeled isatin analog for imaging caspase-3 activation in apoptosis. Bioorg Med Chem Lett 2006;16:5041–5046. [PubMed: 16891117]
201. Haberkorn U, Kinscherf R, Krammer PH, Mier W, Eisenhut M. Investigation of a potential scintigraphic marker of apoptosis: radioiodinated Z-Val-Ala-DL-Asp(O-methyl)-fluoromethyl ketone. Nucl Med Biol 2001;28:793–798. [PubMed: 11578900]
202. Aloya R, Shirvan A, Grimberg H, Reshef A, Levin G, Kidron D, et al. Molecular imaging of cell death in vivo by a novel small molecule probe. Apoptosis 2006;11:2089–2101. [PubMed: 17051335]
203. Cohen A, Ziv I, Aloya T, Levin G, Kidron D, Grimberg H, et al. Monitoring of chemotherapy-induced cell death in melanoma tumors by N,N′-Didansyl-L-cystine. Technol Cancer Res Treat 2007;6:221–234. [PubMed: 17535031]

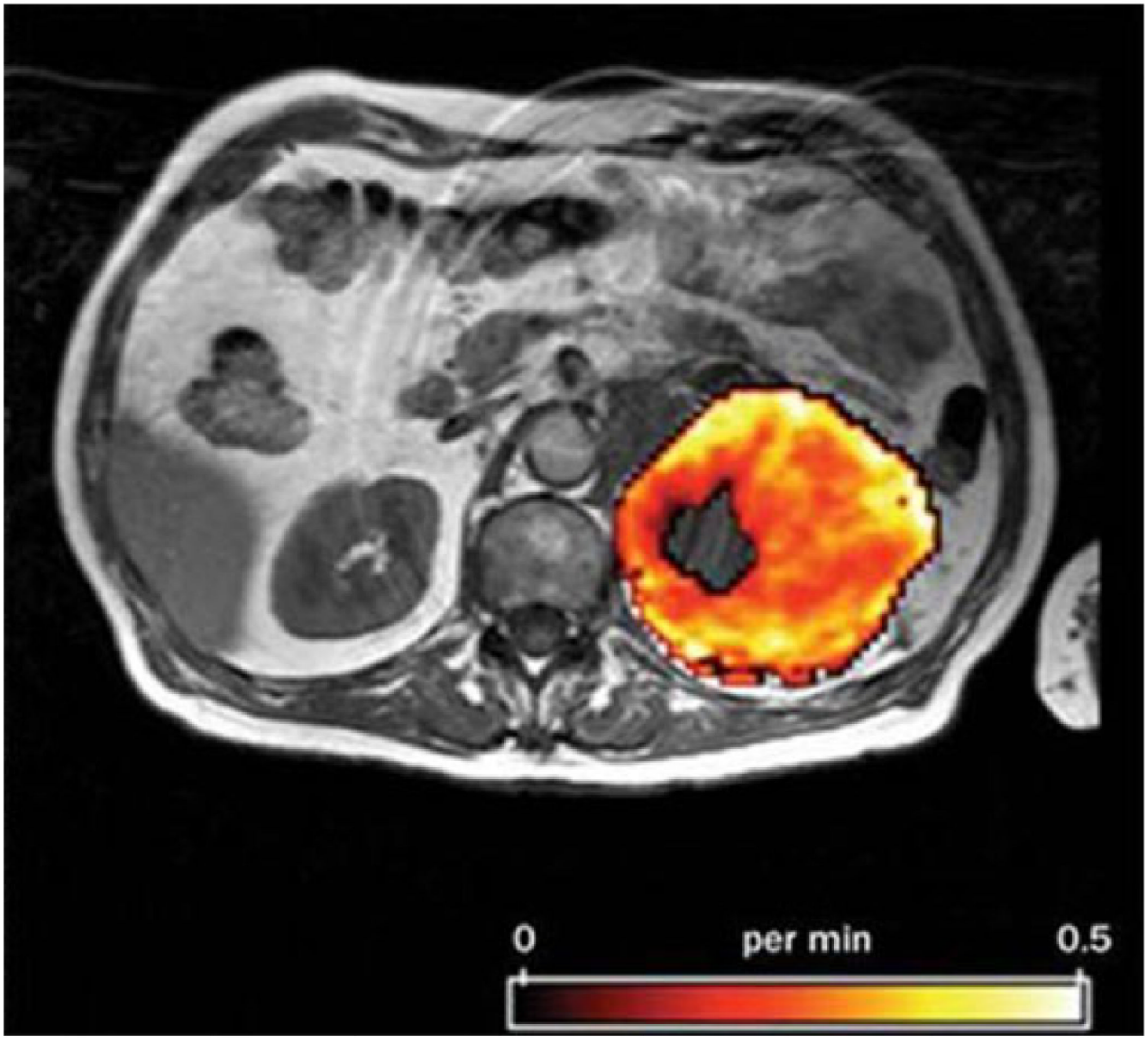

Fig. 1.
Kinetic modeling through DCE is often used to measure K^{trans}, a metric measured in min^{-1} that relates to tumor vessel permeability. Reprinted with permission from Nature [31]

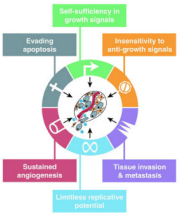

Fig. 2.
Several functions separate neoplastic cells from healthy cells. These differences can be targeted through various molecular imaging methods. Reprinted with permission from Elsevier [41]

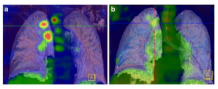

Fig. 3.
a ^{18}F-FDG uptake is seen in the primary lesion and multiple lymph nodes. **b** 14 days after treatment with an EGFR inhibitor shows significant reduction in PET activity, corresponding with a 62% reduction in SUV at previous disease sites. Reprinted with permission from the Society of Nuclear Medicine [50]

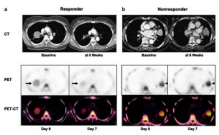

Fig. 4.

a Decreased FLT tumor uptake is seen a week after gefitinib treatment, followed by a CT scan which shows anatomic response after 6 weeks. Similar studies of a nonresponding patient (**b**) show no significant changes after a week after gefitinib. Reprinted with permission from the American Association for Cancer Research [83]

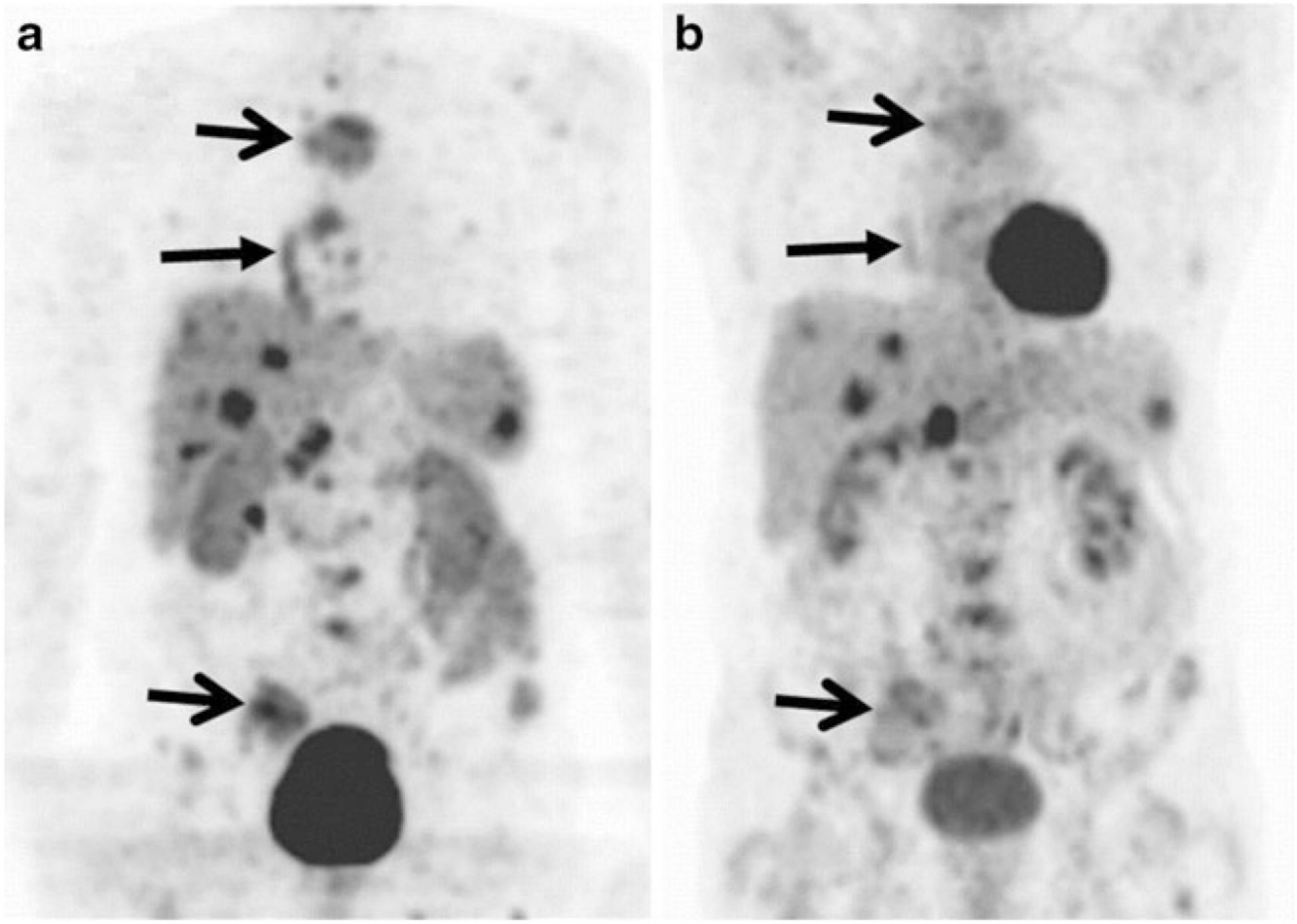

Fig. 5.
A patient's PET with a neuroendocrine tumor primary and multiple metastatic lesions in the liver, spleen, lymph nodes, and bone. Greater enhancement is seen with ^{18}F-galacto-RGD PET (**a**) as compared with ^{18}F-FDG PET (**b**). Reprinted with permission from the Journal of Nuclear Medicine [103]

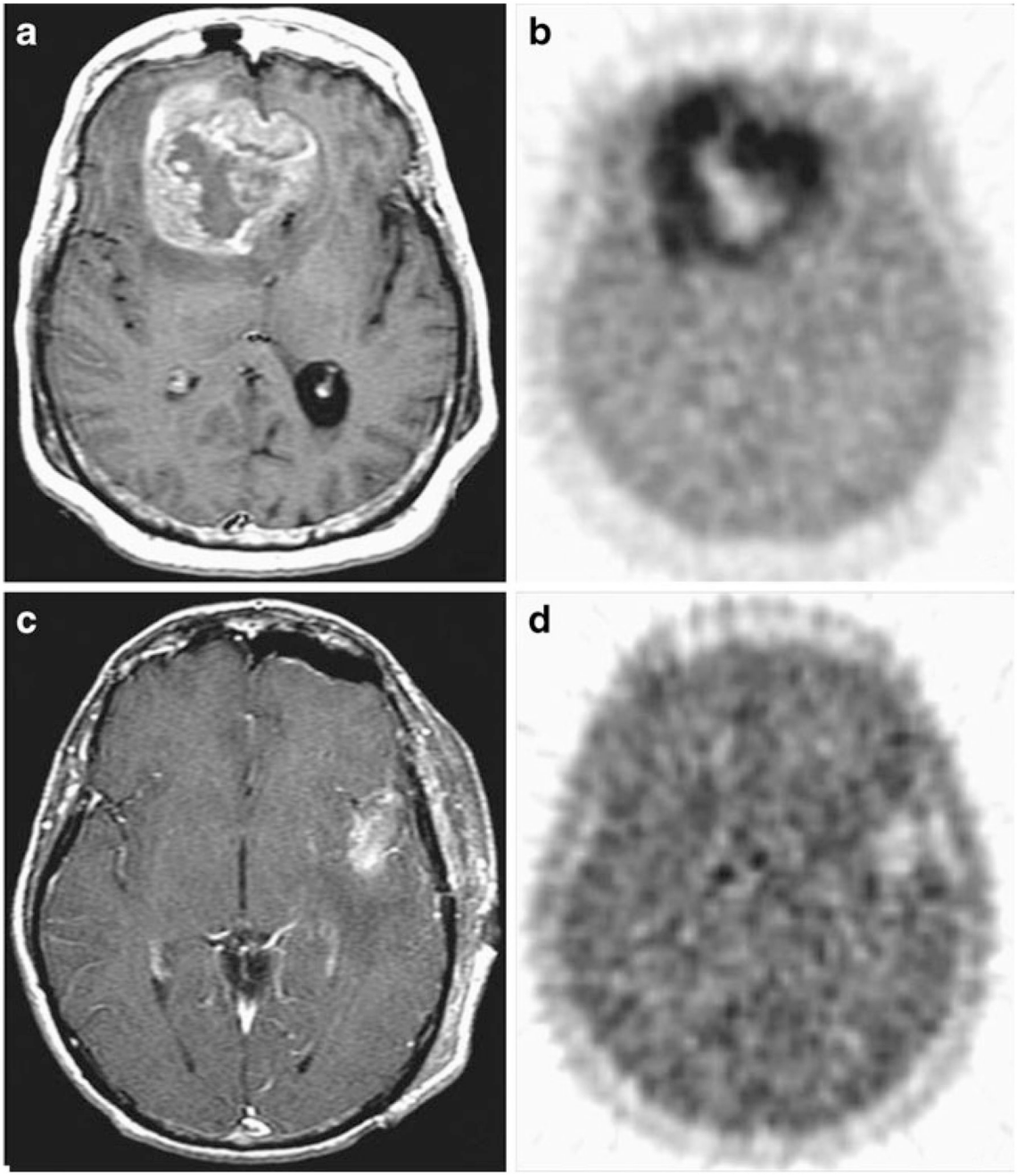

Fig. 6.

a, b A patient with bifrontal glioblastoma multi-forme, with MRI demonstrating a 20 cm^3 mass with a necrotic core, and ^{18}F-FMISO image in the same plane with a T/B_{max} ratio of 3.0. **c, d**A separate patient with left temporal glioblastoma multiforme tumor 7 cm^3 in volume after total gross resection. ^{18}F-FMISO had a T/B_{max} ratio of 1.7. Reprinted with permission from the American Association of Cancer Research [162]

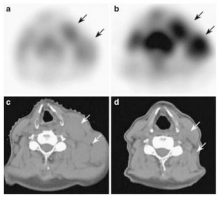

Fig. 7.

Non-Hodgkin's lymphoma in a patient with enlarged lymph nodes of the left neck. Coregistered SPECT and CT images before (**a, c**) and SPECT 48 h after (**b**) low-dose radiotherapy showing a marked increase of labeled annexin V uptake in the tumor. Complete anatomic response is demonstrated in a CT performed 1 month later (**d**). Reprinted with permission from Wolters Kluwer Health [196]